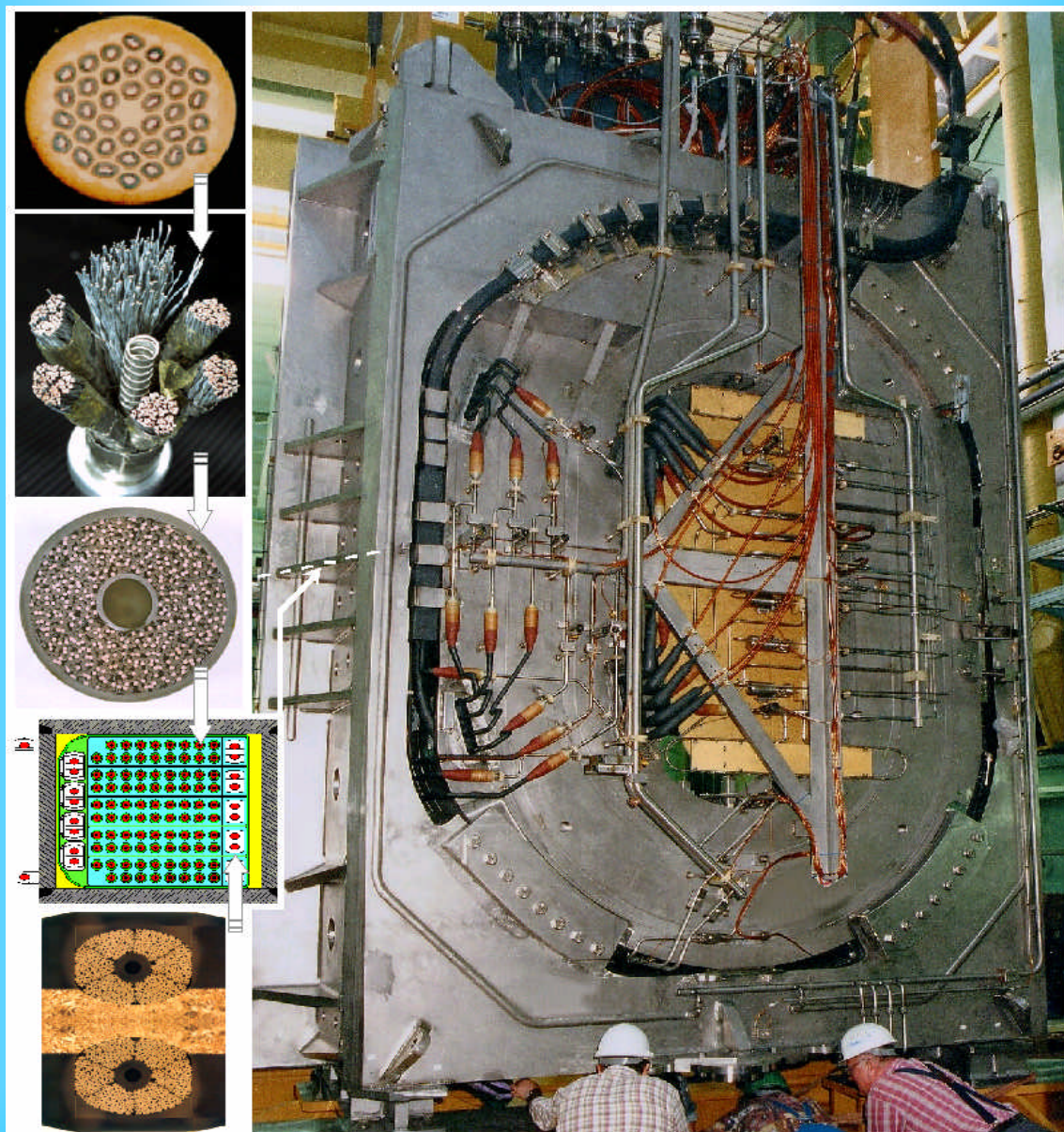


FUSION TECHNOLOGY

Annual Report of the Association EURATOM/CEA 2001

Compiled by : Ph. MAGAUD and F. Le VAGUERES



ASSOCIATION EURATOM/CEA
DSM/DRFC
CEA/CADARACHE
13108 Saint-Paul-Lez-Durance (France)

FUSION TECHNOLOGY

Annual Report of the Association CEA/EURATOM 2001

Compiled by : Ph. MAGAUD and F. LE VAGUERES

ASSOCIATION CEA/EURATOM
DSM/DRFC
CEA CADARACHE
13108 Saint-Paul-Lez-Durance (France)

Tél. : 33 - 4 42 25 46 59
Fax : 33 - 4 42 25 64 21
e-mail : dirdrfc@drfc.cad.cea.fr
Web : <http://www-fusion-magnetique.cea.fr>

This report is also available on-line at : <http://www-fusion-magnetique.cea.fr>

1	6
2	
3	
4	
5	

Cover : Toroidal Field Model Coil (TFMC) installation and test

- 1 – Superconducting strand (courtesy of ENEA)
- 2&3 – Superconducting conductor (courtesy of ENEA)
- 4 – Cross section of the TMFC
- 5 – Superconducting joint
- 6 – TFMC at FZK (courtesy of FZK)

CONTENTS

INTRODUCTION	1
---------------------------	---

EFDA TECHNOLOGY PROGRAMME	3
--	---

Physics Integration

Diagnostics

CEFDA00-561	Support to ITER diagnostic design : polarimetry	5
TW0-DIAG-DEV	ITER diagnostic window development	7

Heating and Current Drive

CEFDA00-553	Support to ITER-FEAT lower hybrid launcher and transmission line	11
CEFDA00-546	Support to ITER ICRF system physics and engineering design - Electrical design of an ICRF array for high RF power density in ITER-FEAT	15
CEFDA00-569	Development of vacuum coaxial capacitors for the ITER-like ICRF JET antenna	19
TW0-ICRF/ANT	ICRF Antenna and vacuum transmission line development - ICRH Antenna coupling : near field computations part II	23
TW1-TPH-ICRANT	ICRF Antenna and vacuum transmission line development - Design & manufacturing of a CW ICRF high power test rig and testing of next step antenna prototype components	29
TW0-NB.DEV.1	Neutral beam development for EDA extension - EU-JA collaborative experiment on KAMABOKO source	31

Vessel/In Vessel

Plasma Facing Components

CNET98-480	Thermal fatigue testing of divertor full scale prototype - 200 kW electron beam gun test	35
CNET98-485	Thermal fatigue testing of baffle full scale prototype - 200 kW electron beam gun test	39
CEFDA00-543	High heat flux testing and analysis of small scale mock-ups - Part 2 : Analysis	43
CEFDA00-565	Improvement evaluation for infrared detection of PFC defects - SATIR upgrading	47
CEFDA01-581	Critical heat flux testing of hypervaportrons - 200 kW electron beam gun test	51

DV4.3	Optimisation and manufacture of high heat flux components - Study of flat tile cascade failure possibility for high heat flux components	53
TW0-DV4/01	Optimisation of manufacture of high heat flux components : tungsten monoblocks	55
TW0-T438-01	Development and testing of time resolved erosion detecting techniques	59
TW1-TVP-MAN1	Optimisation and testing optimisation of CuCrZr/SS tube joints - Optimisation and manufacturing of samples by diffusion bonding	63
Vessel/Blanket		
CEFDA00-556	Simulation of ultrasonic inspection process	67
CEFDA01-587	Study to evaluate ITER proposals for VV code use	71
TW0-LASER/CUT	VV intersector maintenance - Further development of high power Nd YAG laser cutting - Improvement of YAG laser backplate cutting by adding powder ...	73
TW0-LASER/HYD	YAG laser process for cutting and welding of the blanket module hydraulic connections	77
TW0-LASER/REWELD	VV intersector maintenance - Further development of high power Nd - YAG laser rewelding after cutting	81
TW0-LASER/WELD	VV intersector joining - Further development of high power Nd - YAG laser welding with multipass filler wire	85
TW1-TVV-LWELD	VV intersector joining - Vacuum vessel laser assembly	87
T216-GB8	Small scale testing of first wall/shield modules	91
TW0-T420/06	Fabrication of a first wall panel with HIP'ed beryllium armor	93
TW0-T420/08	Development of HIP fabrication technique	99
TW0-T508/04	Development of Be/CuCrZr HIPping technique	103
TW0-T508/05	Development of Be/CuCrCz brazing technique	105
TW1-TVV-HIP	Improvement of HIP fabrication techniques	107
TW1-TVV-ONE	Optimisation of one step SS/SS and SS/CuCrZr HIP joints for retainment of CuCrZr properties	111
Remote Handling		
CEFDA00-524	Study to optimise intersector welding robot (IWR) design and machining characteristics	115
T252	Radiation tolerance assessment of standard components for remote handling and process instrumentation	119
T329-5	In-vessel RH dexterous operations - Task extension 2	125
TW0-DTP/1.1 TW1-TVA-BTS	Carrier and bore tools for 4" bent pipes	129
TW1-TVA-IVP TW0-DTP1.2&4	Prototypical manipulator for access through IVVS penetrations (IVP)	133

TW1-TVA-MANIP	In-vessel dexterous manipulator	137
TW1-TVA-RADTOL	Radiation tolerance assessment of remote handling components	139

Magnet Structure

Cryoplant

CEFDA00-517	Design of cryogenic transfer lines and ring manifolds for ITER-FEAT	143
CEFDA00-566	Layout of the cryoplant for RTO/RC ITER	145

Magnets

CEFDA00-541	Magnet design on PF and correction coils : conceptual design and analysis	147
M40	Design work on magnet R&D	153
M50	Conductor R&D - Development of NbTi conductors for ITER PF coils	157
TW0-T400/01	CSMC and TFMC installation and test	159
TW1-TMC-CODES	Design and interpretation codes	163
TW1-TMC-SCABLE	Cable and conductor characterization	167

Tritium Breeding and Materials

Breeding Blanket

Water Cooled Lithium Lead (WCLL) Blanket

TW1-TTBA-001-D01	Test blanket module - Adaptation to next step machine	169
TW1-TTBA-001-D04	Tritium breeding module adaptation to next step machine - Adaptation of thermal-hydraulic performance to ITER specification	173
TW1-TTBA-002-D01	Blanket manufacturing techniques - Definition of specification of a demonstrator	175
TTBA-2.1	Blanket manufacturing techniques - Definition of specifications for demonstrators	179
TTBA-2.2	Blanket manufacturing techniques - Solid HIP demonstrator for fabrication and coating, fabrication of double wall tubes	183
TW1-TTBA-002-D02	Blanket manufacturing techniques - Solid HIP demonstrator for fabrication and coating, fabrication of double wall tubes	185
TW1-TTBA-002-D03	Blanket manufacturing techniques - DIADEMO experimental program - Results of U bent DWT tests on Pb-Li	189
TW1-TTBA-002-D05	Blanket manufacturing techniques - Integrated mixed-powder HIP fabrication route for TBM with DWT	193
TTBA-3.5	Coating qualification and irradiation tests - Permeation out-of-pile testing	197
TW1-TTBA-004-D03	Processes and components - Blanket neutronic instrumentation	199

TW1-TTBA-005-D02	Safety and licensing : Pb-17Li/water interactions	201
TW1-TTBA-005-D03	Safety and licensing - TBM and TBM system safety	203
TW1-TTBA-006-D02	MHD effects - Test and modelling of natural MHD convection	209

Helium Cooled Pebble Bed (HCPB) Blanket

TW1-TTBB-002-D02	Blanket manufacturing techniques - Mock-up of first wall manufactured with alternative reduced cost fabrication technique	213
TTBB-2.3	Blanket manufacturing techniques - First wall manufacturing by HIP forming technique	217
TW1-TTBB-005-D03	Development of ceramic breeder pebble beds - Characterization of Li_2TiO_3 pebble beds	219
TW1-TTBB-005-D04	Development of ceramic breeder pebble beds - Validation of Li_2TiO_3 fabrication with pre-industrial means of the lab fabrication steps - Mastering/optimisation	223

Structural materials development

Advanced materials

TW1-TTMA-001-D01	SiC-SiC ceramic composite - SiC-SiC composite development and characterization	227
TW1-TTMA-001-D09	SiC-SiC ceramic composite - Joining development : process and mechanical characterization	231

Reduced Activation Ferritic Martensitic (RAFM) steels

TW1-TTMS-001-D02	RAFM steels - Irradiation performance - Neutron irradiation to 30-35 dpa at 325°C	235
TW1-TTMS-002-D03	RAFM steels - Metallurgical and mechanical characterization - Characterization and physical metallurgy	239
TW1-TTMS-002-D04	RAFM steels - Metallurgical and mechanical characterization - Thermal ageing behaviour of EUROFER 97	243
TW1-TTMS-002-D16	RAFM steels - Metallurgical and mechanical characterization - Mechanical properties of diffusion bonded welds (RAFM/RAFM HIP joint)	247
TW1-TTMS-002-D18	RAFM steels - Metallurgical and mechanical characterization - Mechanical properties of HIP powder steel	251
SM-3-3	Corrosion in water conditions (EUROFER 97 and F82H)	253
TW1-TTMS-003-D12	RAFM steels - Stress corrosion cracking in aqueous environments	257
TW1-TTMS-004-D02	RAFM steels - Qualification fabrication processes - Powder HIP processing & specification	259
SM-2-3-1	Mechanical properties of F82H weldments	263
TTMS-2.3.2	Mechanical properties of EUROFER 97 weldments	265
TW1-TTMS-004-D04	RAFM steels - Qualification fabrication processes - EUROFER weldability	267
TW1-TTMS-004-D05	RAFM steels - Qualification fabrication processes - Dissimilar welding with filler	271

TW1-TTMS-004-D06	RAFM steels - Qualification fabrication processes - Solid HIP process qualification, application to complex shapes	275
TW1-TTMS-005-D02	RAFM steels - Rules for design, fabrication and inspection - Design code assessment and development	279
TW1-TTMS-005-D05	RAFM steels - Rules for design, fabrication and inspection - RAFM data collection and data base maintenance	281
TW1-TTMS-006-D01	RAFM steels - Qualification of high performance steels - ODS process and qualification	283
TTMS-6.3.1 TW1-TTMS-006-D03	RAFM steels - Qualification of high performance steels - Microstructure and mechanical properties	287
Neutron source		
TTMI-001	IFMIF - Accelerator facility	291

Safety and Environment

SEA5-1	Validation of computer codes and models	295
SEA5-2	Coherent system of codes for the ITER safety analysis - Validation of computer codes and models	299
TSW-2.1	Waste and decommissioning strategy - Improvement to an existing facility and possibilities for diminishing gas release	301
TSW-2.6	Waste and decommissioning strategy - Requirements of decommissioning and waste management strategies	303
TW0-SEA4 SEA4-4	In-vessel safety - Third set of pre and post calculation of in-vessel LOCA's on the new japanese "ICE" facility	307
TW0-SEA3.5 TW1-TSS-SEA3.5	In-vessel hydrogen deflagration/detonation analysis	311
SEA5.31 TW1-TSS-SEA5	Validation of computer codes and models	313
TW1-TSS-SERF2	Tritium releases and long term impacts	315

System Studies

Power Plant Conceptual Studies (PPCS)

TW0-TRP-3D1	Analyze the sensitivity of achieving accident management	319
TW0-TRP-4D5	In-vessel components	321
TW1-TRP-PPCS1-D04	Model A (WCLL) - Consistency with the PPCS GDRD	325
TW1-TRP-PPCS1-D10	Model A (WCLL) - Design integration	327
TW1-TRP-PPCS3-D01	Selection of advanced models - Assessment of Pb-17Li cooled blanket and divertor concepts using SiC _f /SiC as structural material	331

Socio-economic studies

TW1-TRE-ECFA-D01	Externalities of fusion - Comparison of fusion external costs with advanced nuclear fission reactor	335
TW1-TRE-ECFA-D02	Externalities of fusion accident - Sensitivity analysis on plant model and site location	339

JET Technology

JET-EP-Div	The JET EP divertor project	343
JW0-FT-2.5	Tritium processes and waste management - Dedicated procedures for the detritiation of selected materials	347

<i>UNDERLYING TECHNOLOGY PROGRAMME</i>	349
---	-----

Physics Integration

Diagnostics

UT-PE-HFW	Transparent polycrystalline windows	351
-----------	---	-----

Vessel/In Vessel

Plasma Facing Components

UT-PFC&C-HIP	Mechanical behaviour of HIP joints	355
UT-VIV/PFC-BDG	Boron doped graphites	359
UT-VIV/PFC-SiC/MJ	Development of SiC/metal joining techniques	361
UT-VIV/PFC-W/Coat	Development of thick W CVD coatings for divertor high heat flux components	365
UT-VIV/PFC-TMM	Thermo-mechanical models	369

Remote Handling

UT-VIV/AM-Actuators	Remote handling techniques - Advanced technologies for high performances actuators	371
UT-VIV/AM-ECIr	Remote handling techniques - Radiation tolerance assessment of electronic components from specific industrial technologies for remote handling and process instrumentation	373
UT-VIV/AM-HMI	Remote handling techniques - Graphical programming for remote handling techniques	377
UT-VIV/AM-Hydro	Remote handling techniques - Technology and control for hydraulic manipulator	381

Tritium Breeding and Materials

Breeding Blanket

UT-TBM/BB-IMBLA	Improved breeding blanket	385
UT-TBM/MAT-LM/MAG	Liquid metal corrosion under magnetic field	391
UT-TBM/MAT-LM/Refrac	Compatibility of refractory materials with liquid alloys	395
UT-TBM/MAT-LM/SiC	Compatibility of SiC _f /SiC composites with liquid Pb-17Li	399
UT-TBM/MAT-LM/WET	Wetting of materials by liquid metals	405

Materials development

Structural materials

UT-TBM/MAT-BIM	Dissimilar diffusion-bonded joints mechanical testing	409
UT-SM&C-COR	Metal and oxide thermodynamic stability and solubility in water cooling systems	413
UT-SM&C-LAM/Weld	Laser weldability of LAM steels (Eurofer 97)	417
UT-TBM/MAT-LAM/Mic	Influence of the martensite morphology on the plasticity behaviour of the Eurofer steel	421
UT-TBM/MAT-LAM3	Microstructural investigation of Reduced Activation Ferritic-Martensitic (RAFM) steels by Small Angle Neutron Scattering (SANS)	425
UT-TBM/MAT-Mod	Modelling of the resistance of the dislocation network to the combined effect of irradiation and stress - Comparison of a pulsed and a continuous irradiation on the secondary defects structure in an annealed 316L steel	429
UT-TBM/MAT-ODS	Development of forming and joining technologies for ODS steels	433

Fuel cycle

UT-TBM/FC-SP	Separation of the D/T mixture from helium in fusion reactors using superpermeable membranes - Superpermeation : nonmonotonous energy dependence at low energy ion bombardment and the effect of membrane carbidization on hydrogen permeation through the niobium membrane	437
--------------	--	-----

Safety and Environment

UT-S&E-BLK	Blanket safety – Design of a test section for MHD experimental program	441
UT-S&E-Mitig	Evaluation and mitigation of the risk connected to air or water ingress	443

System studies

UT-SS-REL	Reliability / availability assessment - Double walled tube concept, impact on the pressure tubes reliability / availability	447
-----------	---	-----

<i>INERTIAL CONFINEMENT FUSION PROGRAMME</i>		451
ICF01	Intense laser and particle beams dynamics for I.C.F. applications	453
ICF02	Cryogenic targets production using magnetic levitation	457
ICF03	Laser-matter interaction at relativistic intensities and fast igniter studies	461
ICF04	European collaborative experiment on the fast igniter concept	463
ICF-KiT-PRC	Overview on power reactor concepts	465
<i>APPENDIX 1 : Directions contribution to the fusion programme</i>		469
<i>APPENDIX 2 : Allocations of tasks</i>		473
<i>APPENDIX 3 : Reports and publications</i>		479
<i>APPENDIX 4 : CEA tasks in alphabetical order</i>		491
<i>APPENDIX 5 : CEA sites</i>		497

Task Title : THERMAL FATIGUE TESTING OF DIVERTOR FULL SCALE PROTOTYPE
200 kW electron beam gun test

INTRODUCTION

Thermal fatigue seems to be one of the most important damaging mechanism for the ITER divertor plasma facing components. Therefore, an assessment of the behaviour of its components under cycling heat loads is essential to demonstrate the validity of the selected design solution.

This report presents the 2001 activities on dome prototypes. A final report including 2000-2001 test results (Infrared examination + High Heat Flux testing) on 6 prototypes of ITER divertor (3 straight and 1 curved CFC NB31 monoblocks and 2 curved Tungsten/Copper plasma sprayed prototypes) is available since end of 2001 [1].

2001 ACTIVITIES

TESTING OF DOME PROTOTYPES

Description of the mock-ups

Two V-shapes elements prototypes of the ITER divertor dome were manufactured with the same geometry and mounted in parallel on a mechanical structure allowing connection to the FE200 water loop (see figure 1):

- MCTS-1314 is the lower element and consists in a rear stainless steel support (5 mm) assembled with a heat sink part in Glidcop including Glidcop tubes (OD 12 mm, thick. 1 mm) with internal stainless steel liner of 0.3 mm.

The element was compacted by High Isostatic Pressure (HIP) process at 930°C and then plasma sprayed with a mixed Tungsten/Copper spray. The Tungsten armour was castellated on the lower pressure leg of the mock-up, thickness of the coating is theoretically 3 mm.

- MCTS-1318(9) is identical than precedent one except the fact that the mock-up was compacted with a thick rear stainless steel support machined after HIPping process down to a thickness of 10 mm. There is no castellation on this mock-up.

Thermographic examination (SATIR facility)

Infrared characterisation does not point out strong defects of HIPping (see figure 2).

Note that the surface of the coating is not homogeneous, furthermore, thickness of coating is not constant (see figure 3) and presents some bubbles or holes on the surface.

High heat flux testing (FE200 facility)

3 steps of fatigue cycling were performed on each side of the mock-up:

- 1) 100 cycles at 1 MW/m² removed heat flux into the water.
- 2) 1000 cycles at 2 MW/m² removed heat flux into the water.
- 3) 1000 cycles at 4 MW/m² removed heat flux into the water.

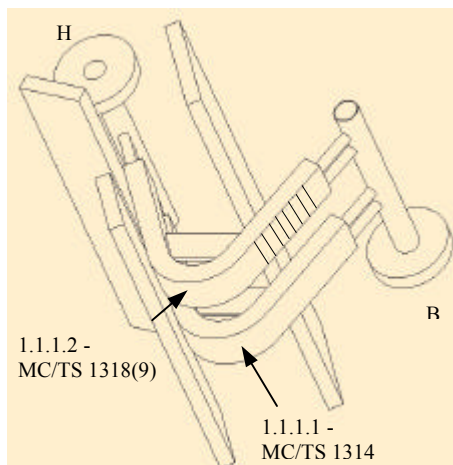


Figure 1 : Sketch (with protection dumps) and view of the mock-up

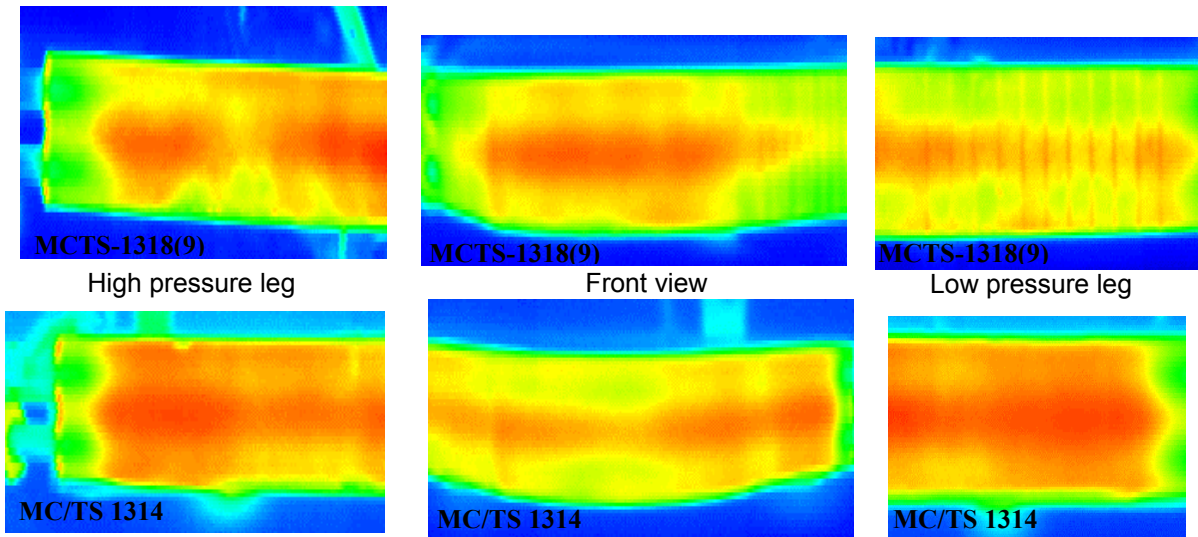


Figure 2 : SATIR view of the sample during transient thermal shock (front view and lateral views)

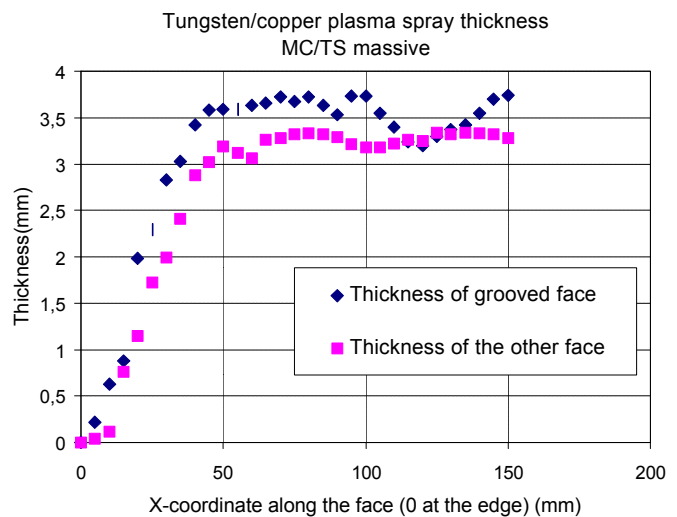
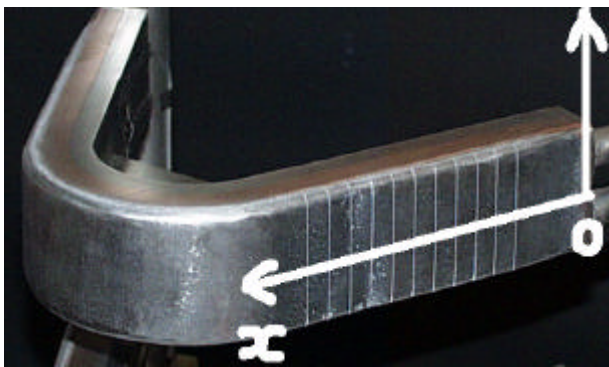


Figure 3 : Example of thickness measurements

Step 1 :

Cycling on the high and low pressure legs of MC/TS massive and MC/TS 1314 allowed a global checking of the testing routine and a optimisation of positioning.

A typical surface temperature of 350°C for a removed flux into the water of 1 MW/m² was attained.

Note that simple thermal calculations from this surprising high value of surface temperature shows that conductivity of tungsten coating is only about 10 % of massive Tungsten. (i.e; around 12 W/mK).

(This result is in accordance with previous tests on plasma spray coating : for the B₄C plasma sprayed on the ergodic divertor neutralizers of Tore Supra, a same value of 10-15 % was found by comparison between conductivities of plasma spray and massive B₄C.)

Step 2 :

A global image of the 4 heated areas during step 2 is given figure 4. Temperature fields are heterogeneous, globally around 600°C (for an absorbed heat flux of 1.8-2 MW/m²), with hot spots up to 700°C.

Nevertheless, the temperature were stable during the cycling step, even after 1000 cycles.

At this moment of the testing campaign, it was decided to start the Step 3 at 3 MW/m² instead of 4 MW/m².

Note that the software emissivity of the optical system was not the same during cycling on high pressure leg and low pressure leg, explaining differences of colour distribution between left and right pictures.

Note also that castellations on the low pressure leg of MC/TS massive are not observable.

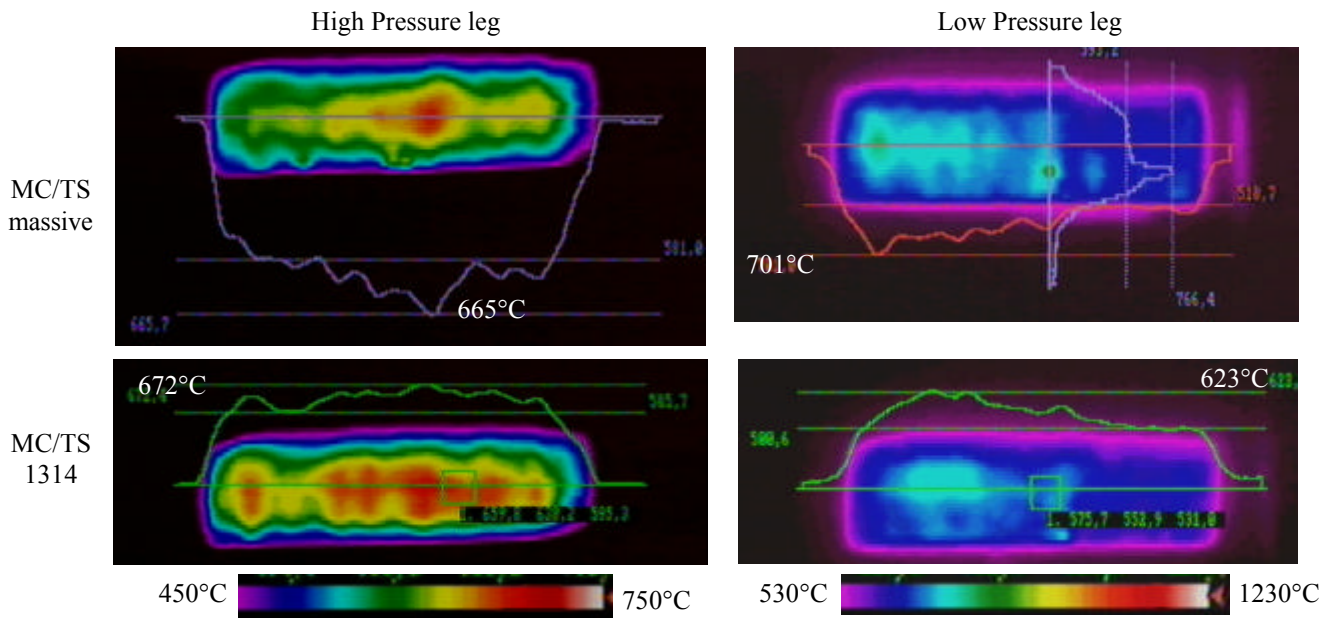


Figure 4 : Global view of the heated areas during cycle 1 of step 2

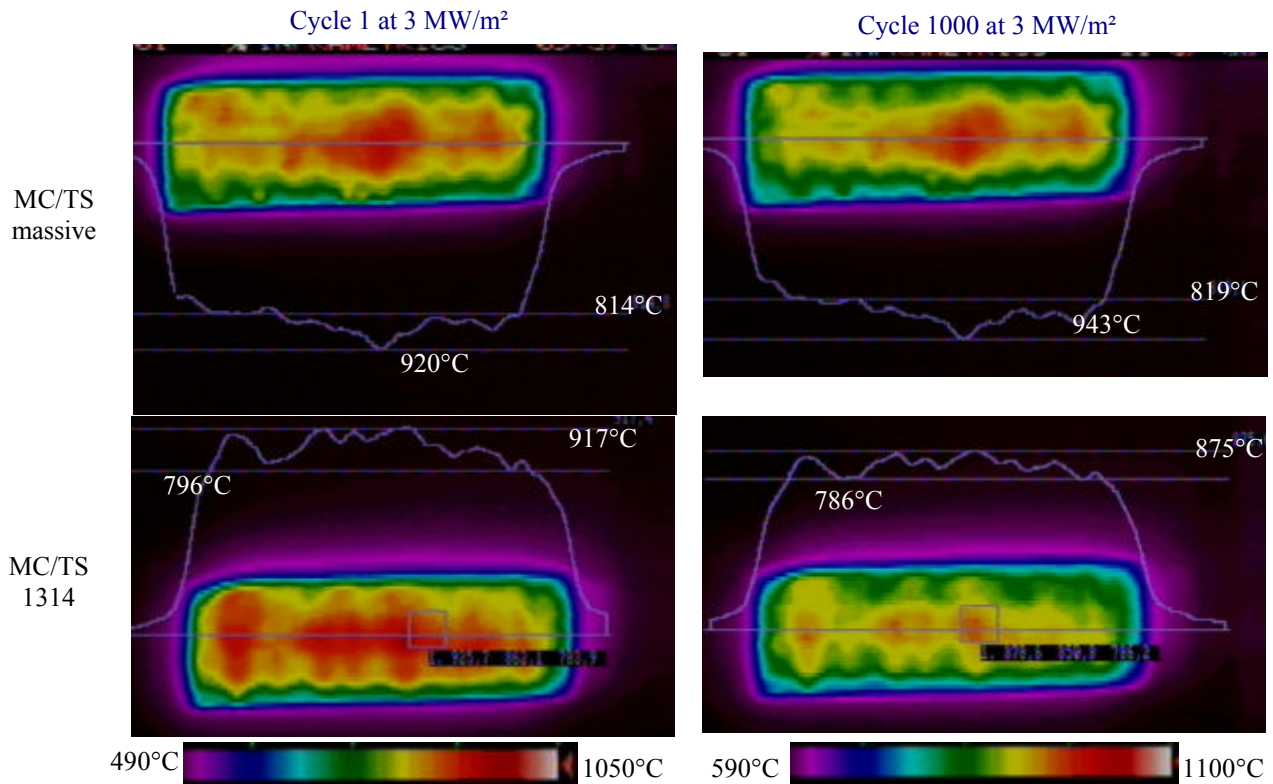


Figure 5 : Low pressure leg of MC/TS massive and MC/TS 1314 before and after 1000 cycles at 3 MW/m²

Step 3 :

a) 1000 cycles at 3 MW/m² were successfully performed on the low pressure leg of the two elements (see figure 5). No difference in the temperature field pattern is observed on the IR pictures. Colours are slightly different due to a slight modification in the range of temperature. Note also that, temperature field pattern being constant, a slight decreasing of temperature can be explained by a power balance fluctuation or an optical transmittance decreasing (pollution of windows for example).

b) As the cycling at 3 MW/m² on the high pressure leg was satisfactory, a tentative screening at 4 MW/m² was performed on the low pressure leg (figure 6a).

During cycling phase at 4 MW/m² on the MC/TS massive mock-up, a hot spot developed on the castellated part up to a visible crack. Cycling was stopped on this component after 874 cycles and continued only on the MC/TS 1314 part up to 1000 cycles without damage (see figures 6b and 7).

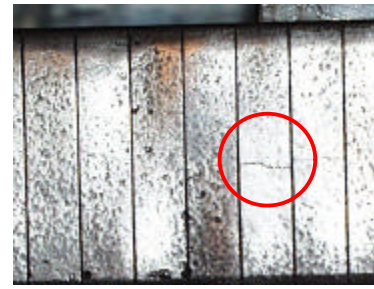
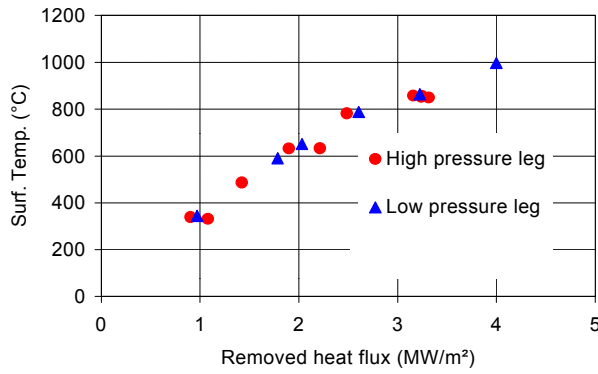


Figure 6a : Screening up to 4 MW/m² (pyrometer on MC/TS 1314, high and low pressure leg) and 6b : crack perpendicularly to castellation after 874 cycles at 4 MW/m²

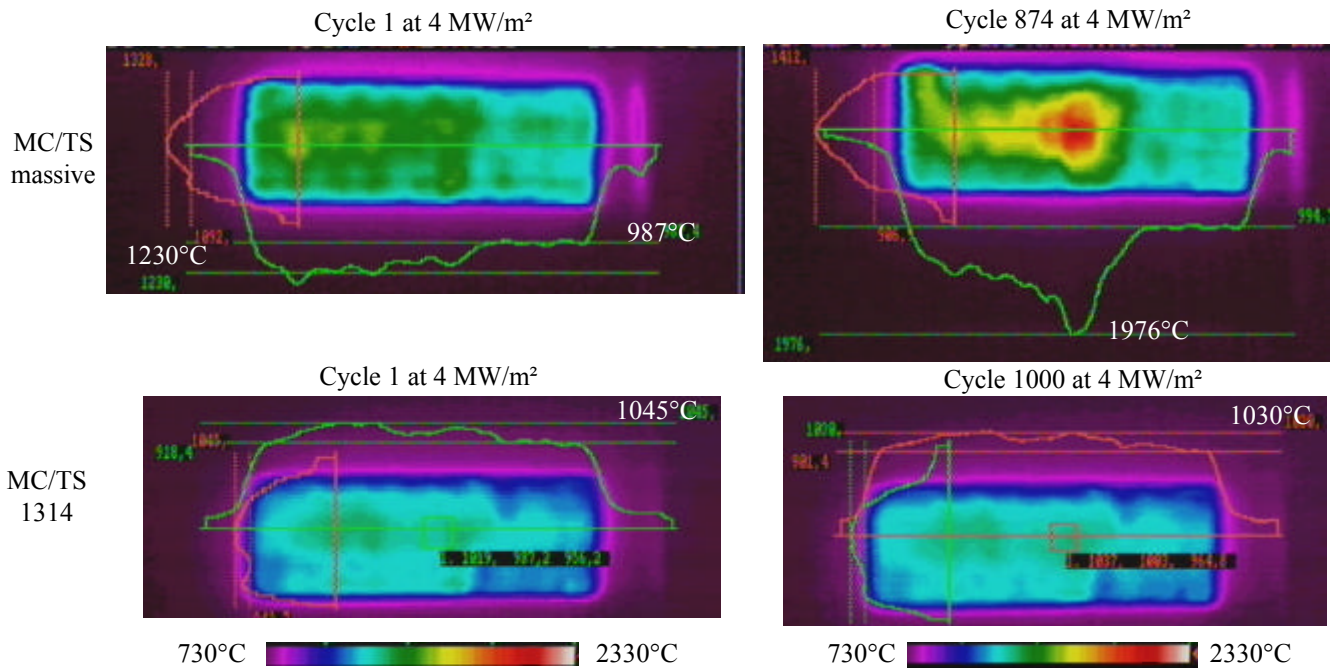


Figure 7 : High pressure leg of MC/TS massive and MC/TS 1314 before and after cycling at 4 MW/m²

CONCLUSION

Two V-shaped elements of plasma Tungsten/Copper sprayed thick mock-ups representative of the ITER dome were high heat flux tested in November 2001 on the FE200 facility in the frame of the NET 98/480 contract with following results:

- conductivity of tungsten coating is only about 10% of massive Tungsten. (i.e; around 12 W/mK),
- operational limit of such plasma spray technology would be 3 MW/m² absorbed heat flux for a surface temperature lower than 1000°C.

REFERENCES

- [1] Contract 98-480 : THERMAL FATIGUE TESTING OF DIVERTOR FULL SCALE PROTOTYPES - FINAL REPORT - CEA CFP/NTT-2001.026 - F. Escourbiac, feb. 2002.

TASK LEADER

F. ESCOURBIAC

DSM/DRFC/SIPP
CEA Cadarache
13108 St Paul Lez Durance Cedex

Tél. : 33 4 42 25 44 00
Fax. : 33 4 42 25 49 90

E-mail : frederic.escourbiac@cea.fr

Task Title : THERMAL FATIGUE TESTING OF BAFFLE FULL SCALE PROTOTYPE
200 kW electron beam gun test

INTRODUCTION

Thermal fatigue seems to be one of the most important damaging mechanisms for the ITER plasma facing components. Therefore, an assessment of the behaviour of any component under cycling heat loads is essential to demonstrate the validity of the selected design solution.

As the manufacturing of the baffle component initially foreseen to be high heat flux tested in the frame of this contract was too much delayed, it was decided, in agreement with European Commission to replace it by a serial of 4 first wall prototypes.

Scope of the contract was to perform thermal fatigue testing on the 4 first wall prototypes in the high heat flux facility FE200.

2001 ACTIVITIES

DESCRIPTION OF THE MOCK-UPS

Two mock-ups respectively named FW5 and FW6 were assembled in CEA and tested in FE200 :

- **FW5** consists in 2 components respectively named PH/S-4K and DS-5Ka mounted in parallel on a mechanical structure connectable to the facility's pressurized water loop, see figure 1.

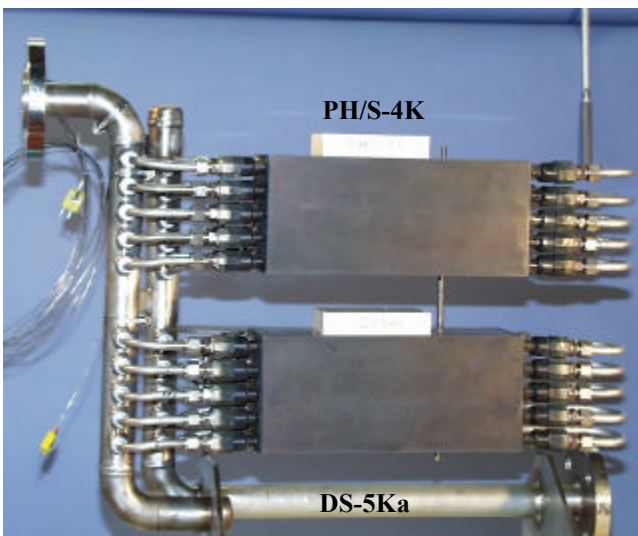


Figure 1 : FW5 = PH/S-4K and DS-5Ka

- **FW6** consists in 2 components respectively named DS-15F and PH/S-6F mounted in parallel on a mechanical structure connectable to the facility's pressurized water loop, see figure 2.

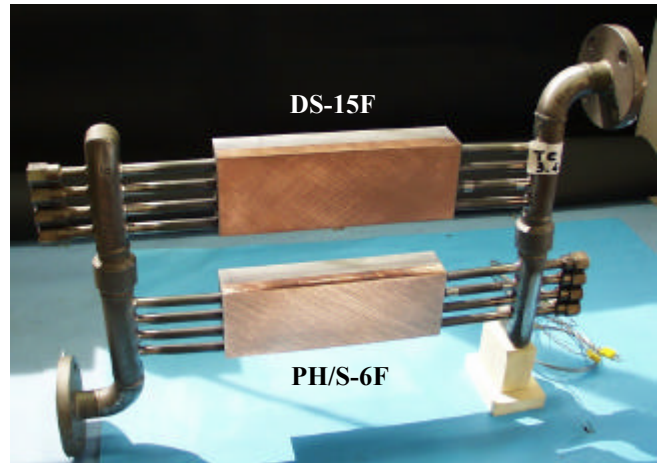


Figure 2 : FW6 = DS-15F and PH/S-6F

A description of each component is given below :

- **PH/S-4K**: made of a 20 mm thick CuCrZr heat sink HIPped at 940°C (2 hours, 140 MPa) onto a 60 mm thick Stainless Steel back plate and tempered at 475°C during 3 hours. The mock-up had 5 Stainless Steel cooling tubes outer diameter 12 mm, thickness 1mm, through the centre of the copper;
- **DS-5Ka**: made of a 20mm thick DS-Copper (IG0) heat sink HIPped at 930°C (2 hours, 140 Mpa) onto a 60 mm thick Stainless Steel back plate (manufactured by Framatome). The mock-up had 5 Stainless Steel cooling tubes outer diameter 12 mm, thickness 1 mm, through the centre of the copper. The cooling tubes were manifolded at the top and bottom;
- **DS-15F**: made of a 20 mm thick DS-Copper (IG0) heat sink HIPped onto a 30 mm thick Stainless Steel back plate. The mock-up had 4 Stainless Steel cooling tubes outer diameter 12 mm, thickness 1 mm, through the centre of the copper. The cooling tubes were manifolded at the top and bottom;
- **PH/S-6F**: made of a 20 mm thick CuCrZr heat sink HIPped onto a 30 mm thick Stainless Steel back plate. The mock-up had 4 Stainless Steel cooling tubes outer diameter 12 mm, thickness 1 mm, through the centre of the copper.

FATIGUE TESTS

Objectives

Aim of the fatigue testing is to induce a damage at the Copper/Stainless Steel HIPped interface. The incident heat flux used in these fatigue tests is much higher than nominal heat flux foreseen in the Next Step machine (1-5 MW/m² instead of < 0.5 MW/m² in ITER) to decrease the number of cycles down to a reasonable value (say ~1000 cycles) leading to defect propagation. Furthermore, ultrasonic (UT) inspection is performed before and after each step of fatigue in order to try to detect the evolution of the damaging process (this second point of interest is not reported here).

Workplan

Table 1 : Foreseen and realized high heat flux tests

		First step of cycling		Second step of cycling	
		Foreseen	Realized	Foreseen	Realized
FW5	PH/S-4K	1000 x 2.5 MW/m ²	yes	1000 x 4 MW/m ²	yes
	DS-5Ka	1000 x 2.5 MW/m ²	yes	1000 x 4 MW/m ²	558 x 4 MW/m ²
FW6	DS-15F	1000 x 5 MW/m ²	yes	1000 x 7 MW/m ²	433 x 7 MW/m ²
	PH/S-6F	1000 x 5 MW/m ²	86 x 5 MW/m ²	1000 x 7 MW/m ²	no

Results

PH/S-4K

a. First step of cycling

The component sustained without any damage the first step of cycling at 2.5 MW/m² (heated area 240 x 100 mm², T_{water} 100°C, 3.6 MPa, ~5 m/s, 10sON/10sOFF). See [1] for details.

b. Second step of cycling

A second step of cycling at 4 MW/m² (heated area 240 x 100 mm², T_{water} 100°C, 3.6 MPa, ~5 m/s, 10sON/10sOFF) was performed on the element PH/S-4K.

This fatigue was supported well with a quite homogeneous surface temperature distribution typically at 600-650°C.

Nevertheless, a probably light damage of the bonded interfaces occurred : Figure 3 shows an increasing of the surface temperature measured by inside thermocouple. A small (around 3 mm diameter) hot spot appeared on the right down corner on IR views and may be detected by ultrasonic testing (see [1]).

DS-5Ka

a. First step of cycling

The component is slightly hotter (420°C compared to 380°C obtained with PH/S-4K) but sustained without any damage the first step of cycling at 2.5 MW/m² (heated area 240 x 100 mm², T_{water} 100°C, 3.6 MPa, ~5 m/s, 10sON/10sOFF).

Right part of the heated area is hotter than the left part since the first screening but no evolution of temperature distribution was observed (+ 25°C systematically between left and right parts). See [1] for details.

b. Second step of cycling

A hot spot developed in the center of the hot right part during the 537th cycle (cf. figure 4), nevertheless thermal fatigue was pursued up to the 558th cycle.

A transient view of the heating during the last cycle gives an accurate view of the debonding area at the plate/tube interface (see [1]).

DS-15F

a. First step of cycling

The component DS-15F sustained the 1000 cycles at 5 MW/m² but developed a slight increasing of surface temperature (cf. figure 5) : + 80°C after 1000 cycles.

A comparison with finite element calculation is proposed Fig. 5: one can check that measured temperature are in good agreement with finite element analysis.

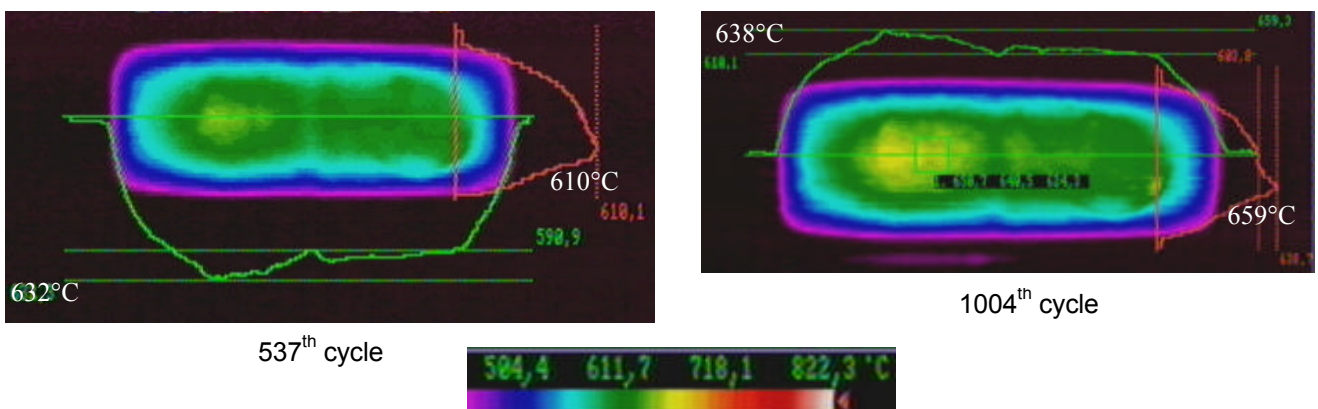


Figure 3 : PH/S-4K under 4 MW/m² absorbed at the 537th and 1004th cycle

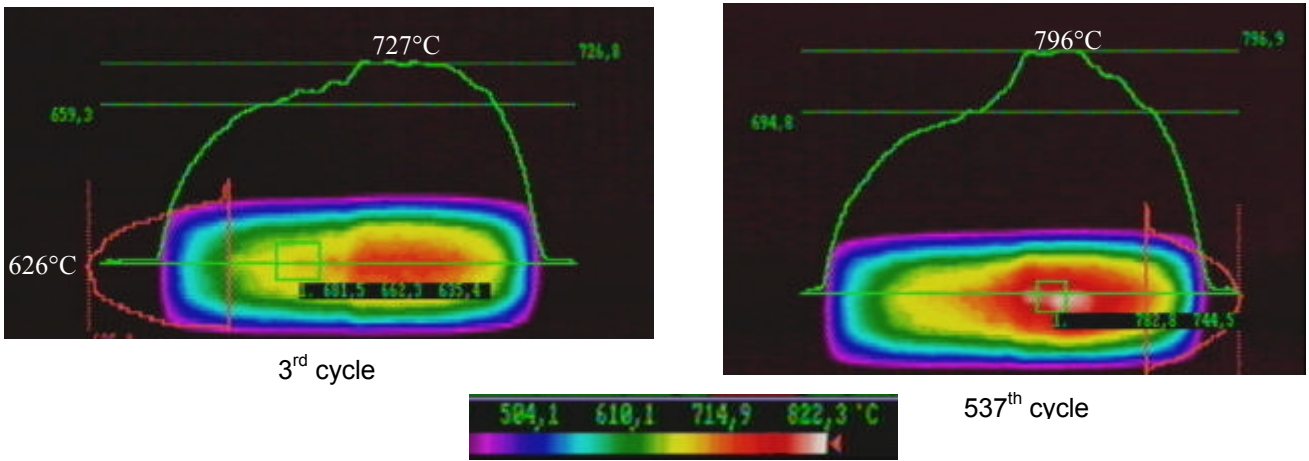


Figure 4 : Hot spot appearance under the 537th cycle at 4 MW/m²

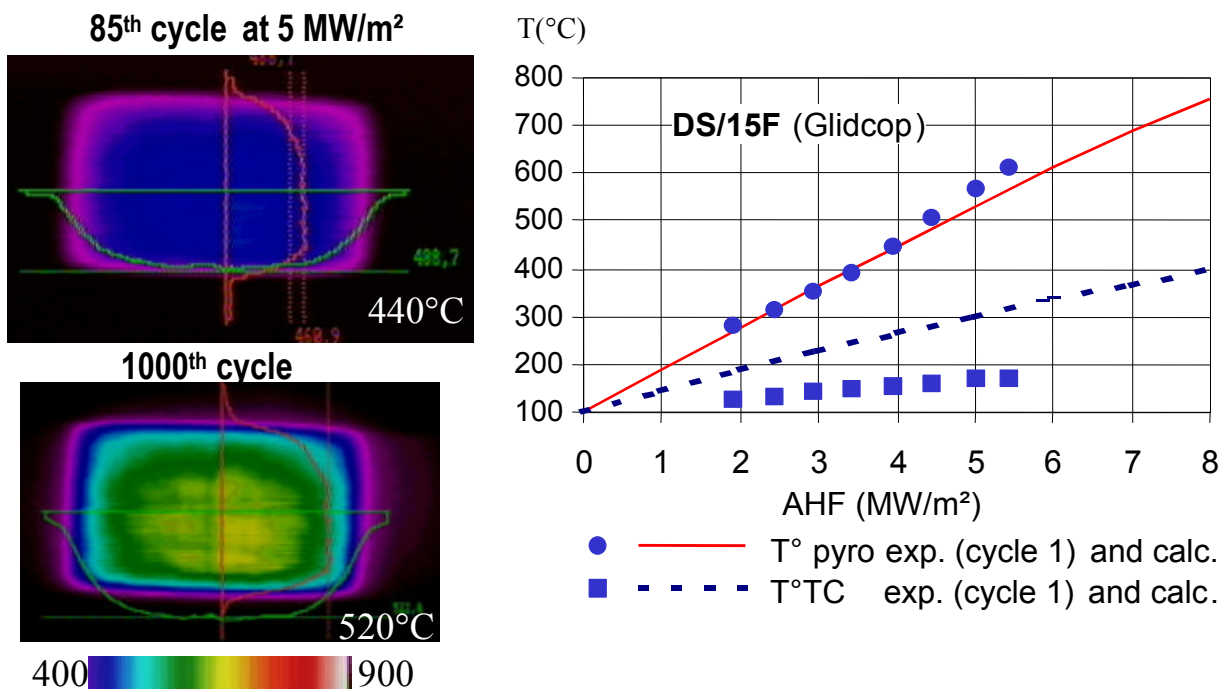


Figure 5 : Infra red view of DS/15F at 85th and 1000th cycle under an AHF of 5 MW/m²
Surface and thermocouple temperature vs AHF compared with Finite Element analysis

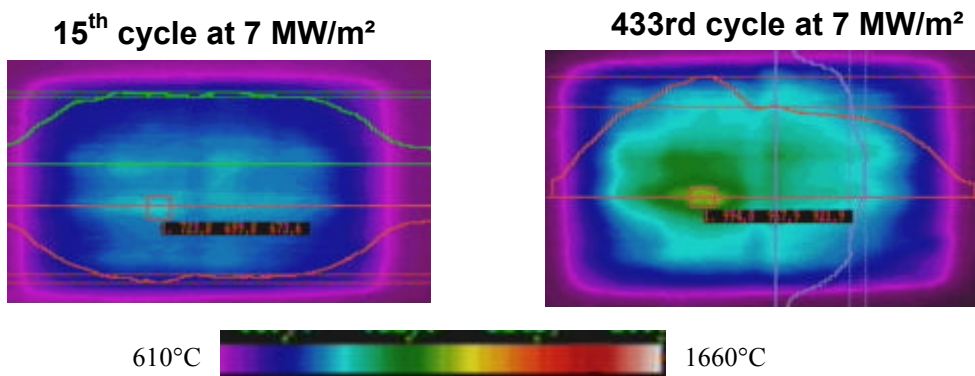


Figure 6 : Development of hot spot at 7 MW/m²

IR monitoring during 70th cycle

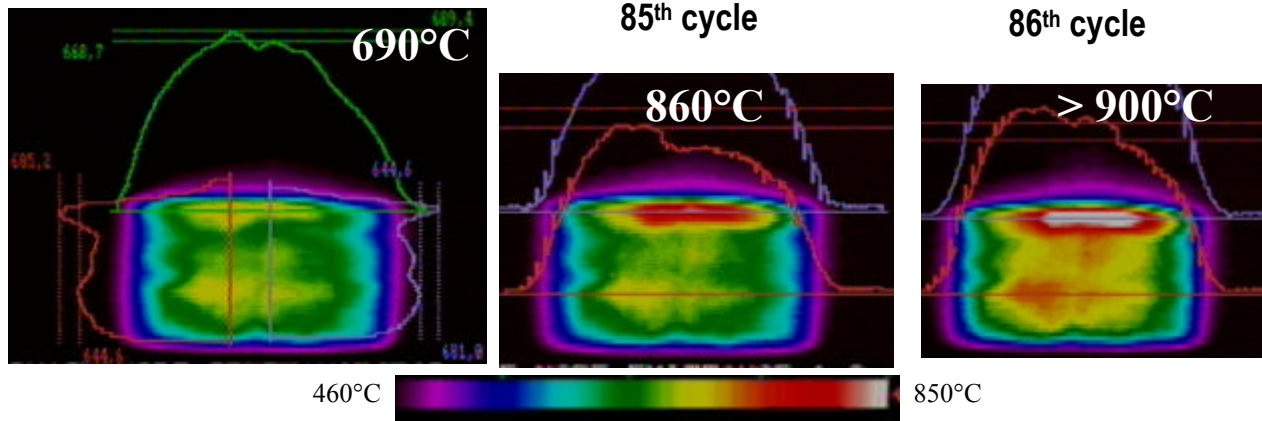


Figure 7 : Evolution of the infra red monitoring during 86th cycle at 5 MW/m²

b. Second step of cycling

A second step of cycling at 7 MW/m² absorbed in the water was performed on the mock-up DS-15F and led to strong interface damage (see figure 6).

PH/S-6F

The mock-up failed during the first step of cycling after 86 cycles at 5 MW/m²: one of the CuCrZr half-shells detached from the other without any water leak, see figure 7.

Naturally, the second step of cycling initially foreseen at 7 MW/m² absorbed in the water was not performed on this component.

CONCLUSION

Four Copper/stainless steel prototypes of ITER first wall were high heat flux tested on FE200 at heat fluxes from 2.5 to 7 MW/m². As foreseen, all of them were damaged by such high fluxes, from a slight increasing of surface temperature (PH/S-4K) after cycling to development of very hot spots (DS-15F, PH/S-6F).

These different degrees of damaging must mainly correspond to HIPed interfaces degradation and have to be correlated with ultrasonic inspection before and after high heat flux tests.

REPORT

- [1] Contract 98-485 : thermal fatigue of baffle full scale prototypes – Final Report
CEA, CFP/NTT-2001.025 – Fev. 2002, F. Escourbiac

TASK LEADER

F. ESCOURBIAC

DSM/DRFC/SIPP
CEA Cadarache
13108 St Paul Lez Durance Cedex

Tél. : 33 4 42 25 44 00
Fax : 33 4 42 25 49 90

E-mail : Frederic.escourbiac@cea.fr

Task Title : HIGH HEAT FLUX TESTING AND ANALYSIS OF SMALL SCALE MOCK-UPS – PART 2 : ANALYSIS

INTRODUCTION

The activities described in this document, performed in the framework of the EFDA Contract 00/543, consist in the analysis (thermal, lifetime evaluation and transient VDE including material melting) of the high heat flux tests performed in the JUDITH facility of several mock-ups supplied by EFDA (Be flat tile, W-macrobrush, W-monoblock and CFC flat tile). For the two last mock-ups, the VDE behaviour has not been tested and analysed. All the calculations have been performed with the CEA finite-elements code CAST3M.

2001 ACTIVITIES

2001 was devoted to the study of the VDE mock-ups, the Be flat tile (see fig. 1) and the W-macrobrush (see fig. 2), with 3 different tile thickness for the first one: 3, 5 and 8 mm, and to the CFC flat tile mock-up. Values of the properties for the considered materials (Be, W1%La₂O₃, CFC-NB31, CuCrZr, Glidcop, OFHC-copper) have been taken from [1]. In elastoplastic analyses, a plastic behaviour with kinematic hardening model was considered for the OFHC, the other materials were assumed elastic. Mechanical analysis were performed using the generalised plane strain mode, bending allowed.

- Pressure is equal to 2.8 MPa.
- Inlet temperature: ambient.

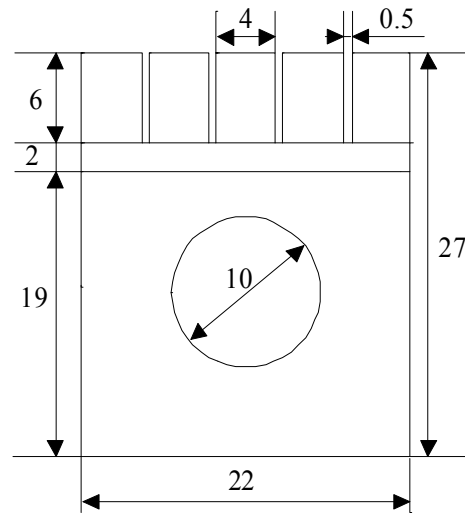


Figure 2 : View and dimensions of the W-macrobrush mock-up

The heat transfer coefficient in the FW water cooling tubes was evaluated according to the CEA recommendations [2]: forced convection regime with the Sieder-Tate correlation, temperature of Onset of Nucleate Boiling obtained with the Bergles and Rohsenow correlation, exchange in the sub-cooled boiling regime with the Thom-CEA correlation, linking of the two regimes through the Bergles and Rohsenow method.

For the VDE simulations, the incident energy was in each case 60 MJ/m² but with different shot duration: 0.1 s and 0.3 s, different heated surfaces, and different assumptions concerning the absorbed power (only 55 % of the input power is absorbed by the mock-up in case of W and 90 % in case of Be). The incident fluxes taken into account in the calculations were therefore varying between 140 and 620 MW/m².

Following [3], a radiation + evaporation cooling occurs at the surface of the tiles at high temperature. This law, giving values of the output flux as function of the surface temperature, has been taken into account in the calculations. The last version of CAST3M is able to take into account melting of materials. Specific thermal model for W1%La₂O₃ and Be was used to computed the melting. Moreover, to take into account the fact that convective motions tend to homogenize the melt layer temperature, the surface material thermal conductivities have been artificially increased to high values above the melting point.

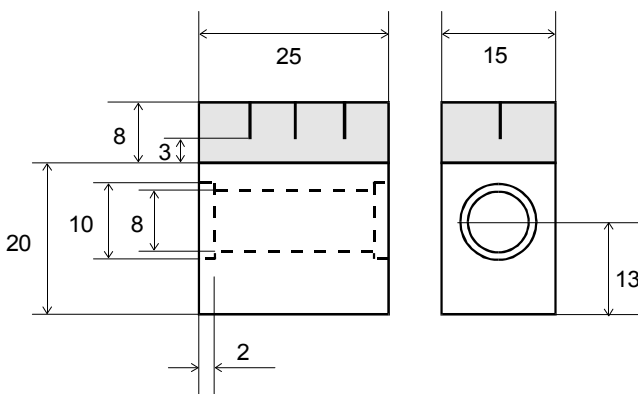


Figure 1 : View and dimensions of the 8mm-thick Be flat tile mock-up

The hydraulics conditions, used during the tests and considered in the analyses, were roughly the same for each mock-up:

- Water velocity of about 13 m/s (then corrected due to the swirl, tape thickness 1 mm and twist ratio = 4) corresponding to flow rates of about 60 l/mn.

Table 1 summarizes the results of the steady state thermal analyses in terms of maximum temperatures obtained at the mock-ups surface. The results of the transient thermal analyses were always in concordance with the steady states ones.

The agreement with the experimentally measured temperatures was also quite good, even if it has been pointed out that it was difficult to obtain during the tests a accurate measurement of the absolute temperature levels. Fig. 3 gives the temperature distribution in the CFC flat tile mock-up for a incident flux of 10.2 MW/m².

Table 1 : Synthesis of the steady state thermal analyses

Mock-up	Inc. Flux	Max. temperature
Be flat tile 3mm-thk	5 MW/m ²	259°C
Be flat tile 5mm-thk	5 MW/m ²	328°C
Be flat tile 8mm-thk	5 MW/m ²	453°C
W-macrobrush	18 MW/m ²	1668°C
CFC flat tile	5 MW/m ²	308°C
CFC flat tile	10.2 MW/m ²	664°C

The results of the VDE calculations are summarized in Table 2. The experimental measured thickness are indicated in brackets.

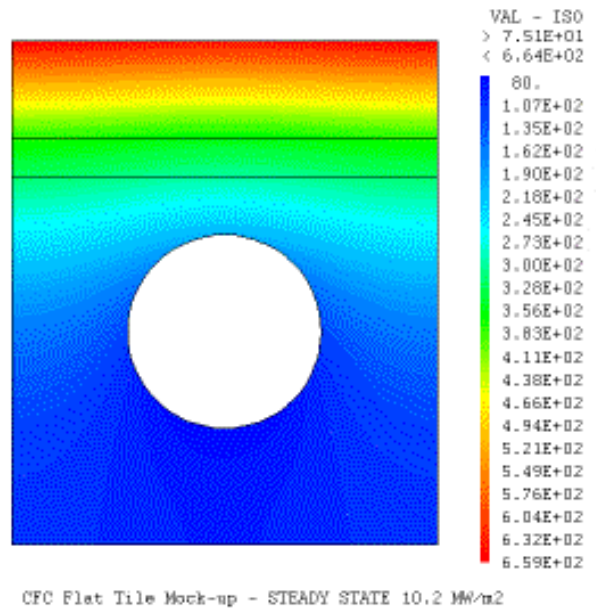
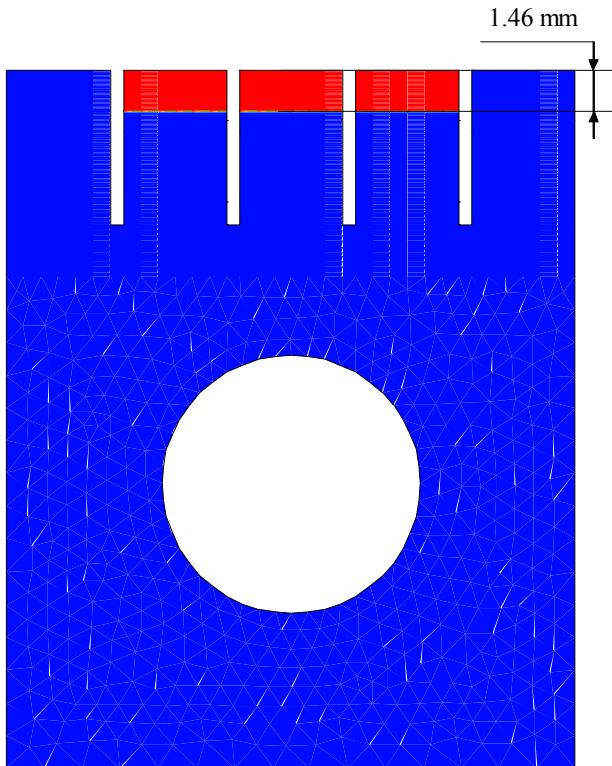


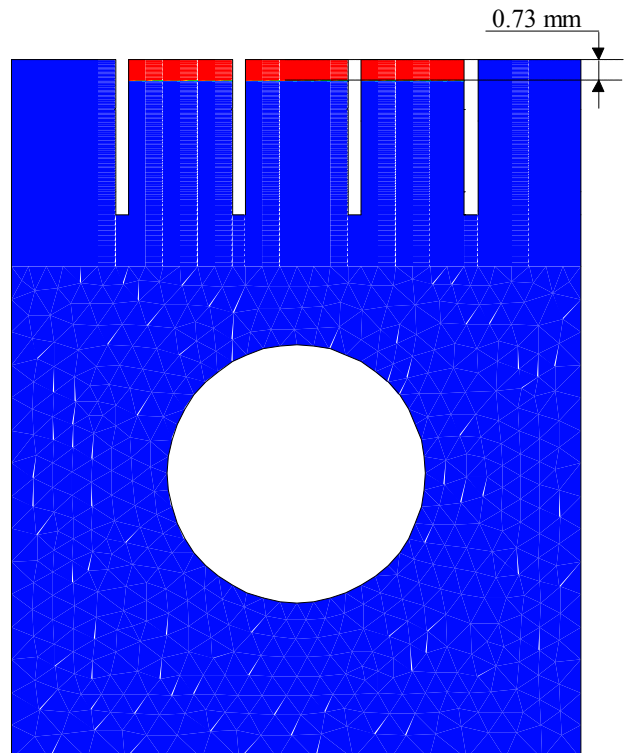
Figure 3 : Temperature distribution in the CFC flat tile mock-up for an incident flux of 10.2 MW/m²

The discrepancies in the case of the W mock-up could be explained by the fact that it was experimentally difficult to well estimate both the input power and the loading time.

The agreement for the Be mock-ups is very good. Fig. 4 shows the calculated melted thickness for the VDE calculations of the W-macrobrush mock-up.



Shot_01 - t = 0.100 s - Melted zone



Shot_03 - t = 0.300 s - Melted zone

Figure 4 : W macrobrush mock-up : VDE calculations : visualisation of the melted zone for both shots

Table 2 : Synthesis of the VDE analyses

Mock-up	60 MJ/m ² for	Melted Thk (mm)
Be flat tile 3mm-thk	0.1 s	2.36 (1.84)
	0.3 s	2.60 (2.46)
Be flat tile 5mm-thk	0.1 s	2.35 (2.45)
	0.3 s	3.00 (2.79)
Be flat tile 8mm-thk	0.1 s	2.56 (2.90)
	0.3 s	3.16 (3.43)
W-macrobrush	0.1 s	1.46 (0.3)
	0.3 s	0.73 (<0.1)

The fatigue lifetime evaluation was based on the level of strain variation obtain in the copper-alloy heat sink for the highest flux transient. Results are given in Table 3.

Table 3 : Synthesis of the fatigue lifetime evaluation

Mock-up	Inc. Flux	$\Delta\varepsilon$ (%)	Nb cycles
Be flat tile 3mm-thk	5 MW/m ²	0.11	> 100000
Be flat tile 5mm-thk	5 MW/m ²	0.13	> 100000
Be flat tile 8mm-thk	5 MW/m ²	0.20	> 100000
W-macrobrush	18 MW/m ²	0.43	~ 40000
CFC flat tile	10.2 MW/m ²	0.35	> 100000

CONCLUSIONS

Steady state and transient thermal calculations, VDE analyses with material melting and fatigue lifetime evaluations have been performed for small scale mock-ups provided by EFDA and tested in the Judith facility.

This comparison experiments/analyses is useful for the interpretation of the phenomena occurring in the tests and will help in the prediction of the HHFC behavior during ITER operation. Moreover, the quite good agreement in the results shows that it is possible to simulate correctly the high heat flux testing.

It has been also pointed out clearly the fact that the precision of the experimental conditions, both input parameters and results measurement, has to be improved.

REFERENCES

- [1] M. Merola, V. Barabash, R. Jakeman, I. Smid, ITER plasma facing component materials database in ANSYS format, ITER doc. G 17 MD 71 96-11-19 W 0.1, Version 1.3, August 2000.
- [2] J. Schlosser, J. Boscary, "Finite Elements Calculations for Plasma Facing Components", Specialist's Workshop on High Heat Flux Component Cooling, Cadarache (September 1993).
- [3] Yu. Igitkhanov, H.D. Pacher, G. Federici, G. Janeschitz, D.E. Post, I. Smid, "Effect of Slow High-Power Transients on ITER Divertor Plates and Limiter Components", 22nd EPS Conf. on Controlled Fusion and Plasma Physics, July 1995, Bournemouth, UK.

REPORTS AND PUBLICATIONS

- [1] J-F. Salavy, F. Picard, High heat flux testing and analysis of small scale mock-ups - Part 2: analysis, CEA report DEN/DM2S SEMT/BCCR/RT/01-022/A, November 2001.

TASK LEADER

Jean-François SALAVY

DEN/DM2S/SEMT/BCCR
CEA Saclay
91191 Gif-sur-Yvette Cedex

Tél. : 33 1 69 08 71 79
Fax : 33 1 69 08 94 26

E-mail : salavy@cea.fr

Task Title : IMPROVEMENT EVALUATION FOR INFRARED DETECTION OF PFC DEFECTS
SATIR upgrading

INTRODUCTION

Infrared thermography is becoming recognised as a technique available today for improving quality control of many materials and structures involved in heat transfer. An infrared thermography test bed named SATIR (Station d’Acquisition et de Traitement InfraRouge) has been developed specially by CEA in order to evaluate the manufacturing process quality of actively water-cooled plasma facing components before their installation in TORE SUPRA (figure 1, figure 2).

The infrared thermography allows characterising the bond between CFC armour tile and metallic heat sink. The quality control of these elements is a necessity to perform high process reliability. SATIR is becoming more and more a valuable tool for detecting cracks and failures. To increase the defect detection limit of the SATIR test bed some technical improvements has been investigated.

2001 ACTIVITIES

Several possibilities have been evaluated to improve the infrared thermography inspection, namely:

- Increasing the DTref value (Treference - Tmeasured).
- Improving the sensitivity and/or resolution of the infrared camera.

- Increasing the flux to the infrared camera.
- Decreasing the noise/uncertainty of the measured surface temperature.
- Reducing the DTref limit.

STUDY OF REPRODUCIBILITY

This study has been performed with Toroidal Pumped Limiter (TPL) component. TPL elements were tested 10 times without modification of any parameters of test bed, such the displacement of infrared camera or the fixation of element tested. Infrared results have been collected during the cooling cycle.

A mean square root average of 0.35°C on DTref was measured. Tests of reproductibility have shown the necessity of SATIR operating procedure more accuracy to control plasma-facing component.

BALANCE OF THE FLOW RATE

A lap of 40 ms between 2 feeding pipes has been checked. The water distribution induces an error of 1°C on DTref measurement.

Feeding pipes of the 3 TPL elements was designed again in order to balance pressure drop distribution and thus flow rate.

Finite elements calculations show that +/-0.05m³.h⁻¹ on the flow rate induces +/-0.5°C on DTref measurement.



Figure 1 : Global view of SATIR

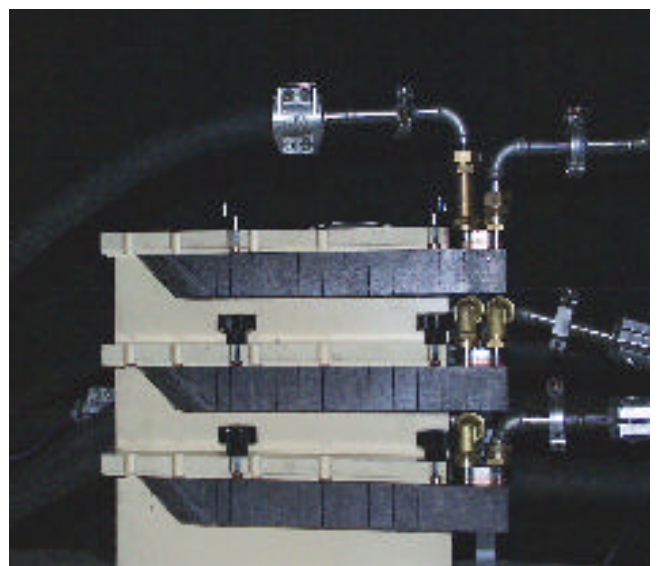


Figure 2 : Plasma Facing Components in testing

MODIFICATION OF THE FLOW RATE

The increasing of flow rate has an effect on heat transfer convective coefficient of the wall pipe. Calculations show that a increasing the flow rate by a factor 3 lead to a increasing of DTref measurement by factor 1.4 (figure 3).

Many problems can be linked with this evolution, especially strong shock inside feeding pipes or faster closing of electro valves.

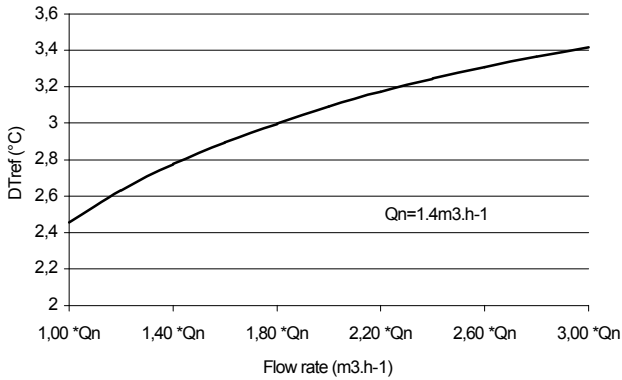


Figure 3 : Flow rate evolution

MODIFICATION OF TEMPERATURE RANGE

A increasing the test temperature range by a factor 2 leads to an increasing of DTref measurement by a factor 2 (figure 4).

To obtain hot water at 160°C it is necessary to pressurize the water loop up to more than 5 bars. In this case the SATIR test bed must conform to the safety standards for pressure vessels. Unfortunately the Signal/Noise ratio could be damaged.

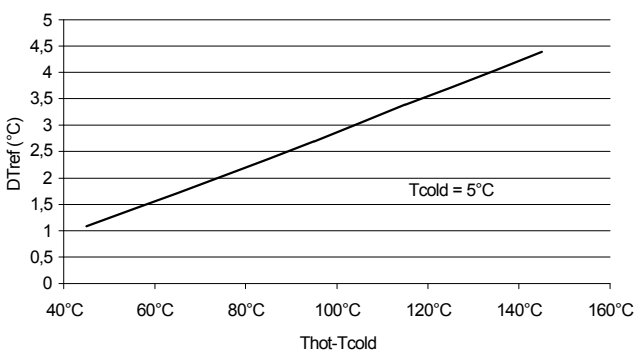


Figure 4 : Temperature range effect

RADIATION SCREEN

Radiation screen has been developed to limit the effect of surrounding radiation (figure 5). 4 groups of 5 tests were carried out: morning and afternoon with radiation screen, morning and afternoon without radiation screen.

The radiation screen allows improving stability of the infrared measurement but only in the case of an important temperature gradient between morning and afternoon.

Presence of the radiation screen divides by 2 the effect of surrounding radiation: 0.4°C variation between a DTref measurement in the morning and in a sunny afternoon, to be compared with a variation of 0.8°C without radiation screen.

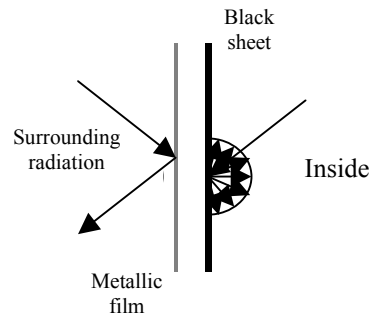


Figure 5 : Radiation screen structure

INFLUENCE OF GEOMETRY

The geometry tolerances and the material property variations play an important role in the determining acceptance criterion.

To quantify the effect of geometry on DTref measurement, a development using finite element code (CASTEM) has been achieved.

In the case of TPL element, the variation of the CFC conductivity of ± 5 % (CFC) leads to a variation of DTref = ± 0.5°C. To respect the geometry tolerance of AMC assembly of ± 0.05 mm, the manufacturer must machine the CFC part or the CuOFHC part.

The variation of the CuOFHC thickness of +0.2 mm (CuOFHC) leads to a variation of DTref = 0.6°C. The variation of the CFC thickness of -0.1 mm (CFC) leads to a variation of DTref = 0.1°C, the variation of copper alloy thickness of ± 0.5 mm (CuCrZr) leads to a variation of DTref = ± 1.7°C

DIGITAL CAMERA

The thermal response depends on the thermal conductivity, the geometry of the different material and the quality of infrared image.

To use digital infrared camera on SATIR test bed a modification of treatment software has been achieved. The quality and spatial stability of infrared image increase with digital camera (figure 6).

- The treatment area is larger of 90 % with numerical camera (detection of edge defect).
- Standard deviation is divided by 2 with the CFC and by 4 with the W tested element.

STATISTIC DATA TREATMENT

A statistic data process based on accumulation of raw data has allowed reducing the global background noise (figure 7).

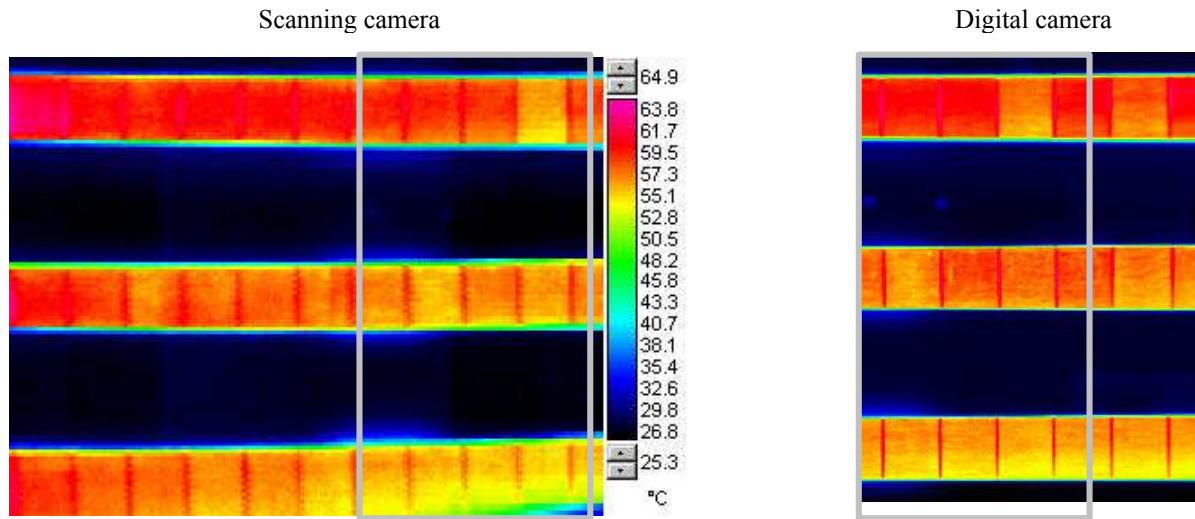


Figure 6 : Infrared image comparison

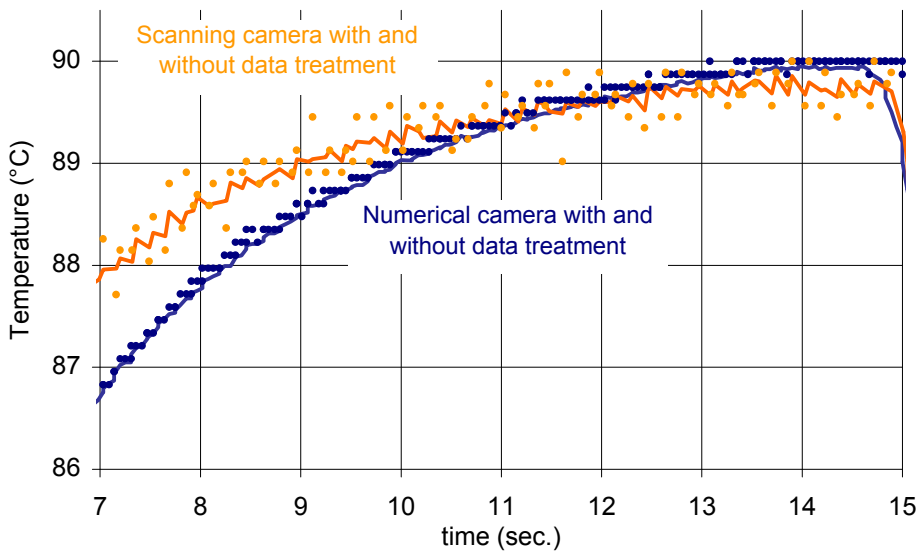


Figure 7 : Statistic treatment of thermal signal

CONCLUSIONS

In order to increase the defect detection limit of the SATIR (infrared test bed) some technical improvements has been investigated (table 1, table 2, table 3). Several possibilities have been evaluated to improve the infrared thermography inspection.

The best defect detection improvement was found with the use of digital camera. By this mean, a sensibility gain of 26 % for W element and 50 % for CFC element has been measured (table 2), the quality, the spatial stability of infrared image and the detection of edge defect have been also improved.

A statistic data process based on accumulation of raw data has allowed to reduce the global background noise by 30 % (table 2). Digital camera detection opens the route for new software improvement which can be studied in the future.

The cost of infrared equipment is estimated at 128Keuros (table 4). Another improvement is by increasing the test temperature range by a factor 2, which leads to a gain of sensibility of 50 % (table 3). In this case the SATIR test bed must conform to the safety standards for pressure vessels. Unfortunately the Signal/Noise ratio could be damaged. This study highlighted the measurement accuracy required for the interface quality control.

Table 1

Experimental action	Measurement
Reproducibility	Standard deviation of 0.35°C
Radiation screen	Allows to improve stability of the IR measure
Balance of the flow rate	Variation $\pm 0.05 \text{ m}^3/\text{h}$ induces $\pm 0.5^\circ\text{C}$
Emissivity deposit	Black coating on W increase e. up to 0.85

Table 2

	Scanning IR camera	Digital camera
CFC element	Standard deviation: 0,46°C	Standard deviation: 0,23°C
W element	Standard deviation: 0,31°C	Standard deviation: 0,08°C
Treatment area	65 %	90 %
Statistic treatment on CFC element	Improving of standard deviation 0.18 to 0.06°C	Improving of standard deviation 0.13 to 0.04°C

Table 3

Finite Elements calculations	Gain
Influence of W monobloc geometry	$\varnothing_i \pm 0.02\text{mm}$ lead to $\pm 0.15^\circ\text{C}$ on DTref
Modification of flow rate	3x Q lead to 1.4xDTref measurement
Modification of range temperature	2x range of temp. lead to 2xDTref measurement

Table 4

Infrared equipment	Cost in kEuro
Digital camera	76
Data acquisition	22
New software development	15
Test bed driving	15

*Total**128*

TASK LEADER

Alain DUROCHER

DSM/DRFC/SIPP
CEA Cadarache
13108 St Paul Lez Durance Cedex

Tél. : 33 4 42 25 62 69

Fax. : 33 4 42 25 49 90

E-mail : alain.durocher@cea.fr

CEFDA01-581

Task Title : CRITICAL HEAT FLUX TESTING OF HYPERVAPOTRONS 200 kW electron beam gun test

INTRODUCTION

Driven by the requirements of ITER machine to reduce costs, there is the need for investigating the possibility of developing cost effective alternatives to the reference design.

One possibility to pursue this objective is replacing the CfC monoblocks tubes in the VT with a hypervapotron CfC flat tile cooling concept.

This solution has the following potential advantages:

- flat tile is cheaper than the corresponding monoblock geometry,
- the width of the VT unit can be increased thus leading to a reduction of the overall number of VT units which has a direct positive impact on costs,
- the difficult transition between the CfC monoblock geometry in the lower half of the VT to the tungsten flat tile geometry in the upper half is avoided,
- flat tile is a more mature technology and is already foreseen in existing tokamaks.

Besides the possible use in the divertor VT, the hypervapotron cooling is now also envisaged in the dome component, the design of which is presently being finalised by the EU Home Team.

Therefore there is a need for consolidating and enlarging the existing hypervapotron critical heat flux (CHF) database also to include the typical cooling conditions of the dome.

The aim of the task is to design, manufacture and test different Hypervapotron (HV) metallic mock-ups in order to consolidate and enlarge the critical heat flux database on this type of geometry.

Tentatively, the following testing parameters are foreseen:

- Three hypervapotron widths: 27 (the present reference width), 40 and 50 mm.
- Three flow velocities are assumed: 4, 7 and 10 m/s.
- Water subcooling: 120 °C.
- Heat flux profile: flat and peaked.

Three critical heat flux tests per set of parameters shall be performed.

Therefore the number of critical heat flux foreseen is: 3 widths x 3 flow velocities x 2 heat flux profiles x 3 tests = 54 tests.

2001 ACTIVITIES

Maximum surface temperature during CHF experiments on FE200 facility will theoretically arise up to 800- 1000°C.

As CuCrZr demonstrated metallurgical instability at high temperature during similar CHF tests in 1996, DS-Copper named Glidcop Al 25 intrinsically more stable at high temperature - from SCM Metal Products, Inc (USA) was preferred to manufacture metallic mock-ups.



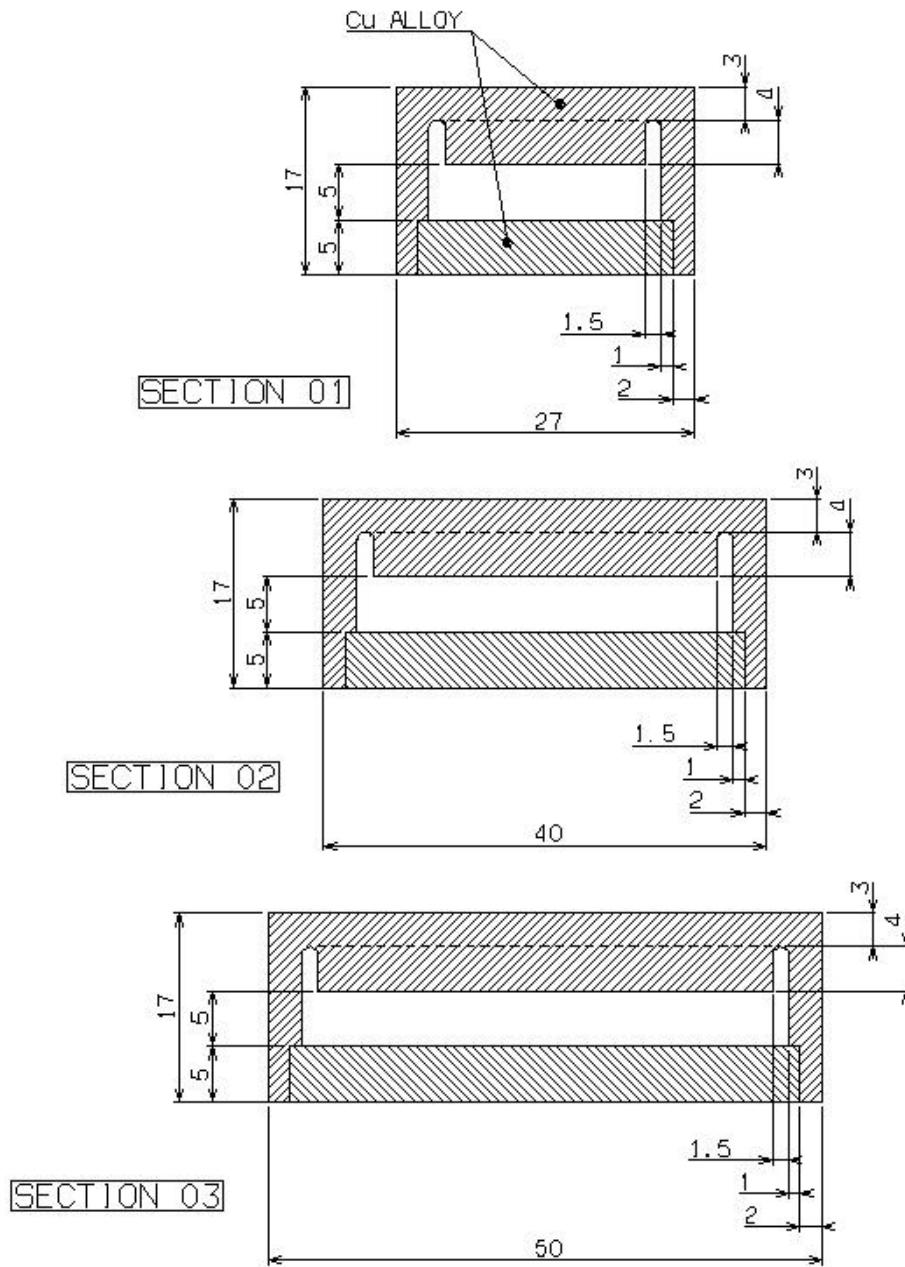
*Photo 1 : State of the machining in 2001
(boxes and rear plugs)*

Machining of the components were completed late in 2001 without specific problems.

Initial design of the 3 sections was respected (sketch 1 and Photo 1) with milling of the transverse teeth into the metallic box.

A step of electron beam welding is now necessary to close the box by welding the rear plug.

This operation will be performed in 2002 before FE200 testing.



Sketch 1 : Design of the 3 initial sections

TASK LEADER

F. ESCOURBIAC

DSM/DRFC/SIPP
CEA Cadarache
13108 St Paul Lez Durance Cedex

Tél. : 33 4 42 25 44 00
Fax. : 33 4 42 25 49 90

E-mail : frederic.escourbiac@cea.fr

Task Title: OPTIMISATION AND MANUFACTURE OF HIGH HEAT FLUX COMPONENTS

Study of flat tile cascade failure possibility for high heat flux components

INTRODUCTION

The object of this task is to evaluate the possibility of failure in cascade of flat tiles under convective heat flux with a glancing incidence. Calculations and tests on the high heat flux (HHF) facility FE200 are foreseen.

Preliminary works in 1999 consisted in the definition of the geometry, the study of the feasibility of the tests by finite elements calculations and the definition of foreseen tests and mock-ups to be prepared.

In 2000 the fabrication of mock-ups were launched in Plansee company, used NS31 (2 mock-ups) and W (2 mock-ups) as armour material and a review of the calculations showed clearly that a chamfering of the tile will be necessary for tests on the FE200. Due to the difficulty to test mock-ups with a glancing incidence it was also decided to test them also under a normal incidence with a peaked profile on one edge in order to simulate the over loading due to a missing tile. The delivery of these mock-ups, first foreseen by end of 2001, is now planned for mid 2002 so that no test was performed in 2001.

2001 ACTIVITIES

RECALL OF THE OBJECTIVES

The flat tile with hypervapotron (HV) cooling has the following advantages:

- It is cheaper than the corresponding monoblock geometry by about 25 % (excluding the armour cost).
- The armour cost is reduced by about 50 %.
- The width of the VT unit can be increased appreciably.
- The surface temperature is more uniform.
- It has a higher critical heat flux limit and a lower pumping power with respect to the "swirl tube" with a twisted tape having a twist ratio of 2.
- A curved component can be manufactured without adding significant manufacturing issues.
- The thickness of the cooling tubes is not intrinsically limited to 1 mm as for the monoblock geometry.

It is worth noting that the cooling tubes represent the only boundary between the pressurised water coolant and the plasma vacuum chambers.

- It is a more mature technology and is already foreseen in existing tokamaks.

However the following issues needs to be investigated:

- It generates significantly higher cyclic thermal stresses than a monoblock geometry; therefore the thermal fatigue lifetime is lower (19 MW/m² x 1000 cycles vs. 24 MW/m² x 1000 cycle for a flat tile and monoblock geometry, respectively). This is particularly important in the bottom part of the VT where the highest heat flux will occur.
- In the case of a convective heat flux, as for the lower part of the VT, one should also take into account that if one tile falls off, the adjacent tile receives an extremely high heat flux localised on its edge as a consequence of the glancing incidence. As a result a rapid temperature rise occurs in the armour - heat sink joint which might seriously damage the joint. The heat flux to the coolant also increases significantly thus causing possible critical heat flux problems.

This last point is the objective of this task.

REMIND OF TESTS DEFINITION

1. The following input parameters will be assumed for the experimental tests:
 - Heat flux normal to the heated surface: 10 MW/m².
 - Angle of incidence of the heat flux: 3°.
 - Coolant conditions: 100 °C, 3.5 MPa, 12 m/s.
2. Two mock-ups will be manufactured with a CFC (SEP NS31) armour (tiles 20 x 27 x 6 mm) and two ones with a W armour (tiles 6 x 6 x 6 mm). The gap between each tile will be ~1 mm.
3. One mock-up with a CFC armour and one with a W armour will be used for the thermal fatigue test (1000 cycles at 20 and 15 MW/m² for the CFC and W armour, respectively).
4. One mock-up with a CFC armour and one with a W armour will be used for the cascade failure test.

Two CFC tiles, located 100 mm from each end of the mock-up, will have a reduced thickness (5 mm instead of 6 mm) to simulate the loss of a tile. To prevent excessive CFC sublimation, the leading edge of one of the adjacent tiles will be chamfered.

A few W tiles, located 100 mm from each end of the mock-up, will have a reduced thickness (5 mm instead of 6 mm) to simulate the loss of a tile.

5. The study on the possible cascade failure will be performed in two ways: (a) applying a heat flux normal to the surface which simulates the computed heat flux through the pure Cu interlayer, (b) applying a heat flux with a glancing incidence of 3°.
6. The mock-ups will be instrumented with 6 thermocouples each, 3 located in the armour and 3 in the heat sink.

CONCLUSION

The preliminary calculations in 1999 and 2000 have shown that in case of the falling of a tile, one can expect a plasma shaping of the adjacent tile so that the surface temperature is below 2200°C and a stopping of the erosion. But the probability of a failure of the second tile before the end of shaping is very high. Even if it will be difficult to reproduce the exact condition on the FE200 this will be investigated by tests.

The mock-ups are now in fabrication and the test are foreseen for 2002.

TASK LEADER

J. SCHLOSSER

DSM/DRFC/SIPP
CEA Cadarache
13108 St Paul Lez Durance Cedex

Tél. : 33 4 42 25 25 44
Fax. : 33 4 42 25 49 90

E-mail : jacques.schlosser@cea.fr

Task Title : OPTIMISATION OF MANUFACTURE OF HIGH HEAT FLUX COMPONENTS : TUNGSTEN MONOBLOCKS

INTRODUCTION

This task is devoted to the fabrication of tungsten monoblocks mock-ups. Such actively cooled components are candidate for the upper part of the outer vertical target of the ITER FEAT divertor, which curvature is about 0.5m.

They are composed of a CuCrZr heat sink tube, a Cu OFHC compliant layer and tungsten tiles. In this work, attempts to manufacture such complex design using Hot Isostatic Pressing have been made.

In 2000, the CuCrZr/Cu OFHC joining process has been significantly improved compared to previous work [1].

Furthermore, as attempts to define a simple HIP canning system failed [2], a set of machined tools were defined.

2001 ACTIVITIES

MOCK-UP FABRICATION

In 2001, several mock-ups, including straight and curved ones, have been successfully manufactured (figures 1-2).

The process includes a first HIP cycle at high temperature to joint the tiles to the compliant layer and a second HIP cycle at low temperature to joint CuCrZr to Cu OFHC.

As the CuCrZr is used in the as-quenched condition, the low temperature HIP cycle corresponds to an ageing treatment.

The final hardness of the alloy is 128HV1. After HIP, the canister is machined and the tools are removed.



Figure 1 : DS-Cu, W tiles straight mock-up (n° 4)

Among the three curved mock-ups, one failed due to a leak in a weld during HIP and one other had to be repaired for the same reason.

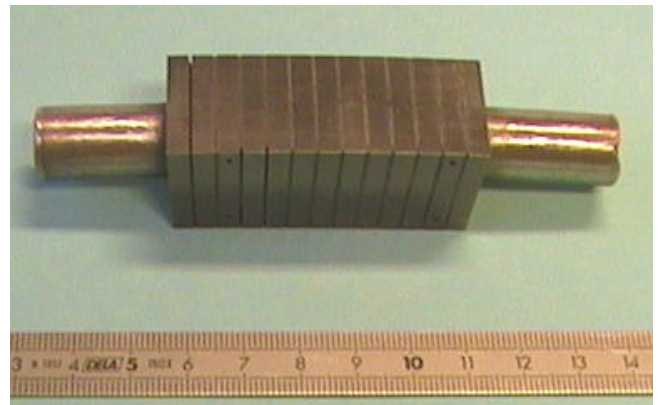


Figure 2 : CuCrZr, W tiles curved mock-up (n° 7)

A description of the mock-ups is given in table 1. Mock-ups 1 and 2 are prototypes manufactured with molybdenum tiles. The Mo/Cu OFHC joints are shown in figure 3. Mock-ups 3 and 4 are straight versions made with tungsten tiles. The reparation consisted in applying again a low temperature HIP cycle, which resulted in over-ageing of the CuCrZr alloy : its hardness decreased down to 87HV1.

Table 1 : List of manufactured high heat flux mock-ups

Mock-up n°	Tiles	Heat sink	HIP	NDT
1 (straight)	Mo	CuCrZr	(950°C, 2h) + (550°C, 2h)	(used for metallography)
2 (straight)	Mo	CuCrZr	(950°C, 2h) + (550°C, 2h)	No defect
3 (straight)	W-1%La ₂ O ₃	CuCrZr	(950°C, 2h) + (550°C, 2h)	Defect at tile 10
4 (straight)	W-1%La ₂ O ₃	DS-Cu	950°C, 2h	No defect
5 (curved)	W-1%La ₂ O ₃	CuCrZr	(950°C, 2h) + (550°C, 2h)	No defect
6 (curved)	W-1%La ₂ O ₃	CuCrZr	Failed	Not tested
7 (curved)	W-1%La ₂ O ₃	CuCrZr	(950°C, 2h) + (550°C, 2h) + repaired at (600°C, 2h)	No defect after reparation

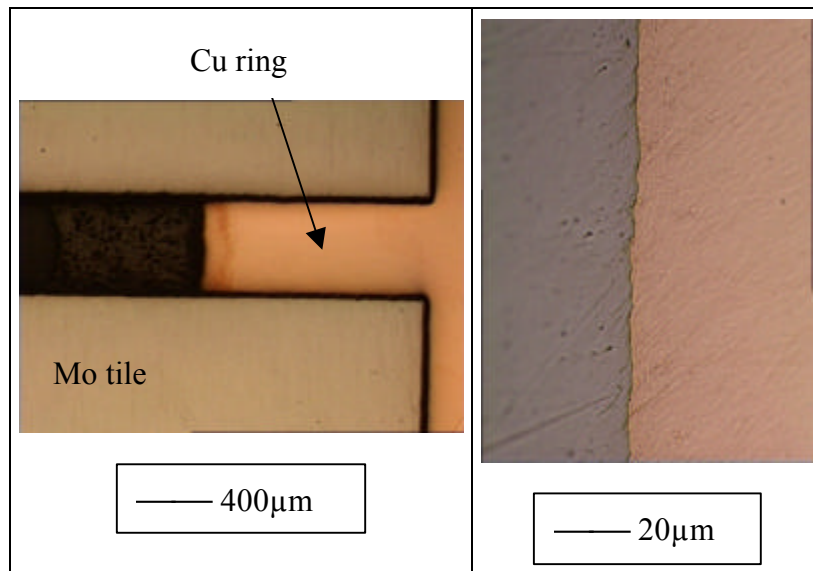


Figure 3 : Mo/Cu OFHC joints, mock-up n° 1

MOCK-UP CONTROL AND TESTING

The mock-ups were controlled by CEA/DRFC using the SATIR thermography installation [3].

Excepted the tile no. 10 on mock-up n° 3 (figure 4), no significant defect could be detected, even on the repaired mock-up.

Mock-ups 2-5 and 7 were sent to Forschungszentrum Jülich for high heat flux testing in the Judith facility.

The test results are summarised in table 2. Excellent results were obtained with the straight Mo/CuCrZr since, the maximum heat removal capacity was limited only by the Mo damage.

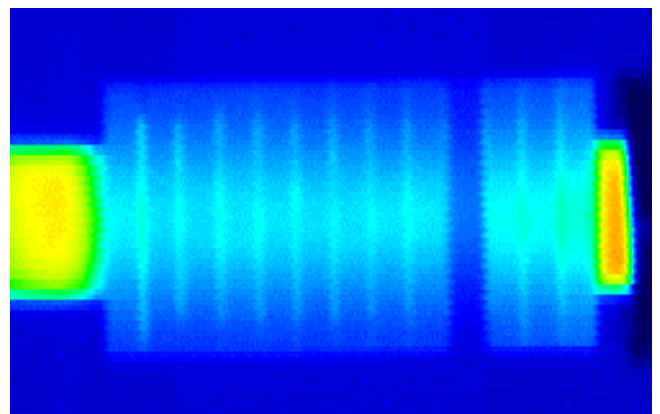


Figure 4 : Infrared image of the "plasma side" of mock-up n° 3, showing a defective tile

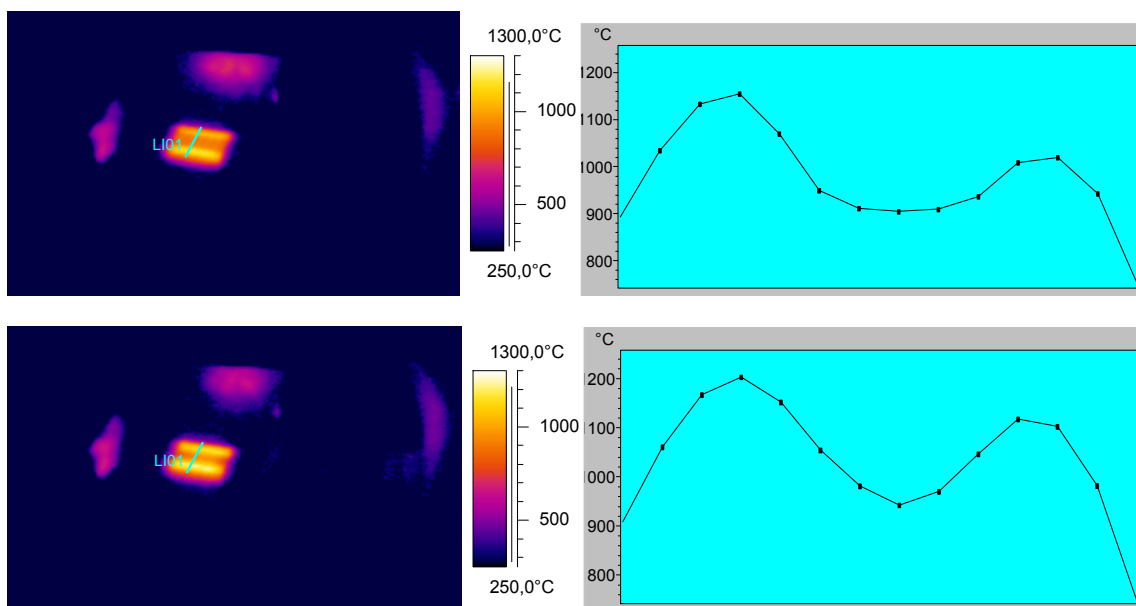


Figure 5 : Temperature profile across a tile from mock-up n° 4 under testing at 18MW/m² absorbed heat flux (32.8MW/m² incident). Top : cycle n° 1, bottom : cycle n° 1000

Excellent results were obtained, too, with the straight W-1%La₂O₃/DS-Cu mock-up (figure 5), that withstood 1000 cycles under a very high heat flux without significant changes in the surface temperature profiles (i.e. no significant joint damage).

Table 2 : Behaviour of monoblock mock-ups under HHF testing

Mock-up	Number of cycles at estimated absorbed heat flux	Results
2	500 cycles at 11.9MW/m ² (13 tiles)	OK
	500 cycles at 22.4MW/m ² (tiles 4 to 9)	Melting and crack formation
4	1000 cycles at 9.6MW/m ² (13 tiles)	OK
	500 cycles at 15MW/m ² (tiles 4 to 9)	OK
	1000 cycles at 18MW/m ² (tiles 4 to 9)	OK (figure 5)
5	1000 cycles at 9.6MW/m ² (13 tiles)	OK
	254 cycles at 15MW/m ² (tiles 4 to 9)	OK
	1000 cycles at 18MW/m ² (tiles 4 to 9)	Increase of surface temperature
7	Screening at 2.8 to 8.3MW/m ² (13 tiles)	Failure at 8.3MW/m ²

The curved W-1%La₂O₃/CuCrZr mock-up n° 5 was slightly less performing than mock-up n° 4 since an increase of the surface temperature was noticed during cycling at 18MW/m² absorbed heat flux.

Results achieved with mock-up n° 7 showed that the reparation was not successful, despite NDT did not reveal any defect.

CONCLUSIONS

Seven tungsten and molybdenum monoblock mock-ups were manufactured using HIP diffusion welding. Mock-ups were controlled using infrared thermography and tested under high heat flux. Very good results were obtained.

REFERENCES

- [1] E Rigal, “Full scale manufacturing of high heat flux components for divertor modules”, ITER task DV4, CEA Report NT DEM 69/98, 4 dec. 1998.
- [2] E Rigal, “Optimisation of manufacturing of high heat flux components for ITER divertor”, interim report task TW0-DV4/01, CEA Report NT DEM 88/2000, 27 nov. 2000.
- [3] N Bommensatt, rapport de contrôle qualité CFP/RCQ-2001.007, CEA/DRFC/SIPP, 11 june 2001.

REPORTS AND PUBLICATIONS

E Rigal, C Grandjacques, F Bruchon “Optimisation of manufacturing of high heat flux components for ITER divertor”, CEA Report NT DTEN n°62/2001, 28 june 2001.

TASK LEADER

3/4 3/4 3/4 3/4 3/4 3/4 3/4 3/4 3/4 3/4 3/4 3/4 3/4 3/4 3/4 3/4 3/4 3/4 3/4 3/4

Emmanuel RIGAL

DRT/DTEN/SMP/LS2M
CEA Grenoble
17, rue des Martyrs
38054 Grenoble Cedex 9

Tél. : 33 4 38 78 97 22
Fax : 33 4 38 78 54 79

E-mail : emmanuel.rigal@cea.fr

Task Title : DEVELOPMENT AND TESTING OF TIME RESOLVED EROSION DETECTING TECHNIQUES

INTRODUCTION

Carbon based material is widely used as plasma facing component in present fusion device due to its good thermophysical properties. This is also the material that has been retained for the ITER divertor. Nevertheless, physical and chemical sputtering yield of carbon are important and induce high erosion rate. The large carbon source reacts with the plasma and creates a very complex Plasma Wall Interaction physic. One of these phenomena, known as redeposition occurs when carbon atoms or ion return to the wall: Due to the reactivity with hydrogen, carbon layers are built up with a large hydrogen content. In the case of ITER, the tritium retention in these carbon redeposited layers may limit the operation for safety reason.

Although erosion and redeposition of carbon may reduce the life time of the divertor tiles and reduce the operation efficiency, only basic measurements have been undertaken in present tokamaks and none of them can provide in situ in a fusion device a time resolved erosion/redeposition measurement. Thus, we develop a technique aiming to measure the erosion and the redeposition process : Speckle interferometry has been retained as the most promising technique and will be tested on the limiter in Tore Supra. In the framework of the CIEL program, it is planed to obtain in Tore Supra high performance long time discharges (up to 1000s). On such a duration, erosion of plasma facing components may become very significant. For a 1000 second discharge, the resulting gross erosion on the LPT in CIEL would be of about $10^{20}C$ per cm^2 or $10 \mu m$. From previous measurements on actively cooled carbon limiter on inner wall in Tore Supra [1], the net erosion rate could be reduced by 2 orders of magnitude. As a consequence, the erosion and redeposition process to measure should be in the range from 0.1 to $10 \mu m$ for a single discharge.

2001 ACTIVITIES

First experiments have shown the feasibility of such technique on a carbon fibre material and provided qualitative and quantitative information on surface displacement. It has also been shown previously [2] that 2 wavelengths are required for a tokamak application. By using a second laser, it is possible to measure the relative displacement and to perform a shape measurement of the object to analyse.

In collaboration with Institut Fresnel in Marseilles, we measured the reflection coefficient on fresh carbon fiber composite (CFC) tiles and on graphite tiles exposed to plasma in Tore Supra.

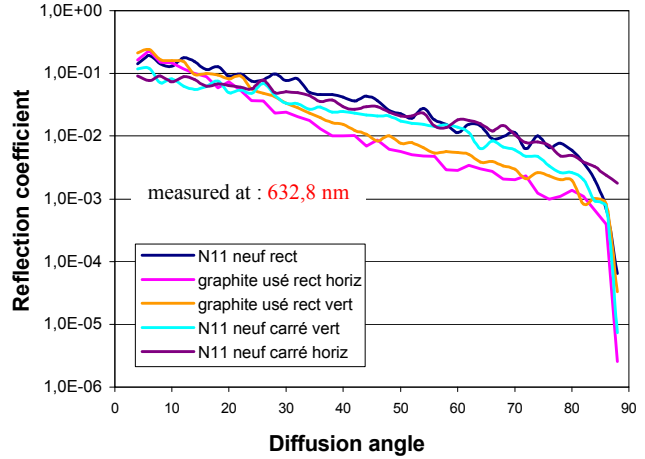


Figure 1 : Reflection coefficient for fresh CFC tile and graphite tile covered with redeposited layer

The reflection coefficients, plotted versus the angle of emission on figure 1, show the same behaviour for both materials; the exposed tiles covered with redeposited layer being slightly more reflective than the unexposed tiles.

According to the proposal made last year, speckle interferometry measurements with 2 wavelengths have been performed with the setting shown on figure 2.

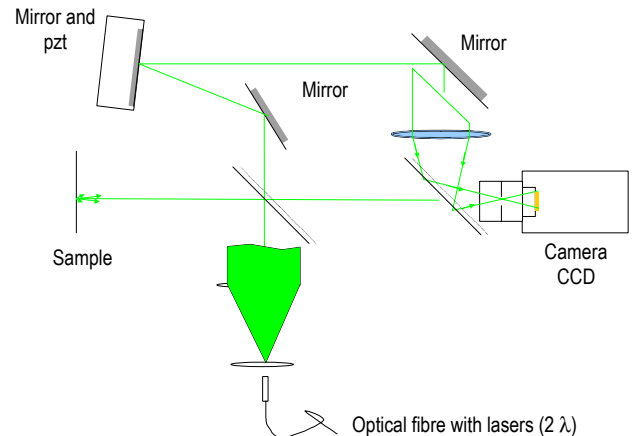


Figure 2 : Experimental set-up for the 2 wavelengths speckle experiments

The two wavelengths used were $\lambda_1 = 532 \text{ nm}$ from a YAG laser and $\lambda_2 = 514 \text{ nm}$ from an argon laser. Phase shifting technique with 4 phases has been used for each wavelength. From the eight pictures acquired, we calculated the phase images plotted on figure 3a. In order to simulate an erosion, we removed a thin layer of $35 \mu m$ on a part of the surface. The resulting phase image is plotted on figure 3b. By differentiation of these two images, it is possible to obtain the phase image plotted on figure 3c, showing the eroded area.

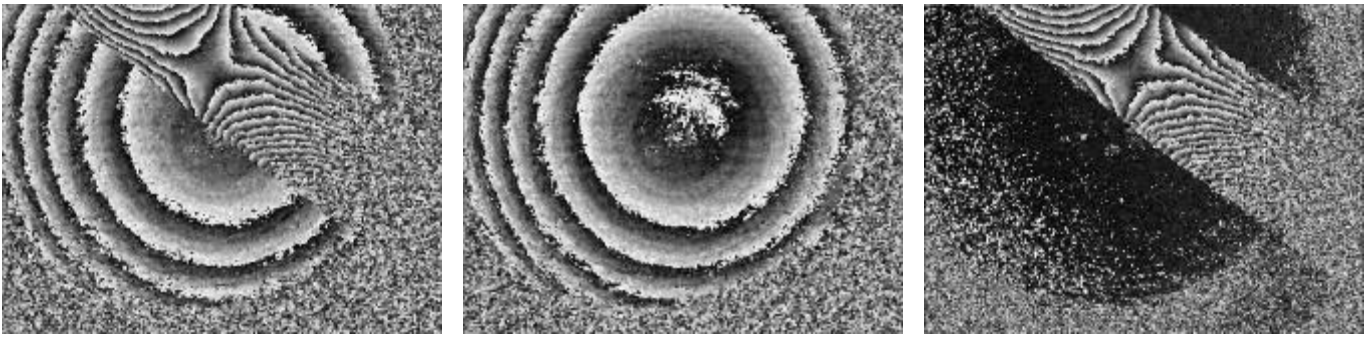


Figure 3 : a) Phase image of a sample with a 35µm layer -
 b) Phase image of the sample without the layer - c) Difference of the phase image

Although, qualitative results were obtained, no quantitative measurements could be performed with this setting. Due to the values of the wavelengths produced by the YAG and argon lasers, the synthetic wavelength, $\Lambda = \frac{\lambda_1 \cdot \lambda_2}{|\lambda_1 - \lambda_2| \cdot \cos\theta}$ equal in that case to 15 µm, was not appropriate to measure erosion in the range of 35 µm. The displacement (or erosion) at the surface being larger than the synthetic wavelength on a pixel size, the lack of correlation between the 2 different states does not allow to extract quantitative information.

In order to overcome this problem, it has been proposed to use an accordable laser, composed with a Yag and OPO laser, allowing to modify continuously the synthetic wavelength from about 0.5 µm to several hundred of micrometers.

Then, we had to face the problem of the large linewidth that is inherent with such lasers.

Experiments performed in collaboration with Marseille University with a 50 cm⁻¹ linewidth OPO has confirmed that Speckle interferometry measurements could not be obtained with such a laser. OPO with linewidth in the range of 0.03 cm⁻¹, designed for interferometry, can be found on the market but the price is larger than the budget allowed by a factor of 2. Therefore it has been decided to buy all the optical components required for the Speckle diagnostic but to postpone the choice of the laser until further tests could be performed. The equipment has been delivered at Cadarache and is installed in a clean room where it is being used. The specifications of the lasers are now defined and experiments with these lasers are in preparation in collaboration with a CEA laboratory in Paris.

In November, an oral presentation has been done by G. Roupillard at a conference hold by the Societe Francaise d'Optique in Tregastel. A modified design of the erosion/redépotion diagnostic based on 2 wavelengths Speckle interferometer and OPO laser has been proposed and is shown on figure 4.

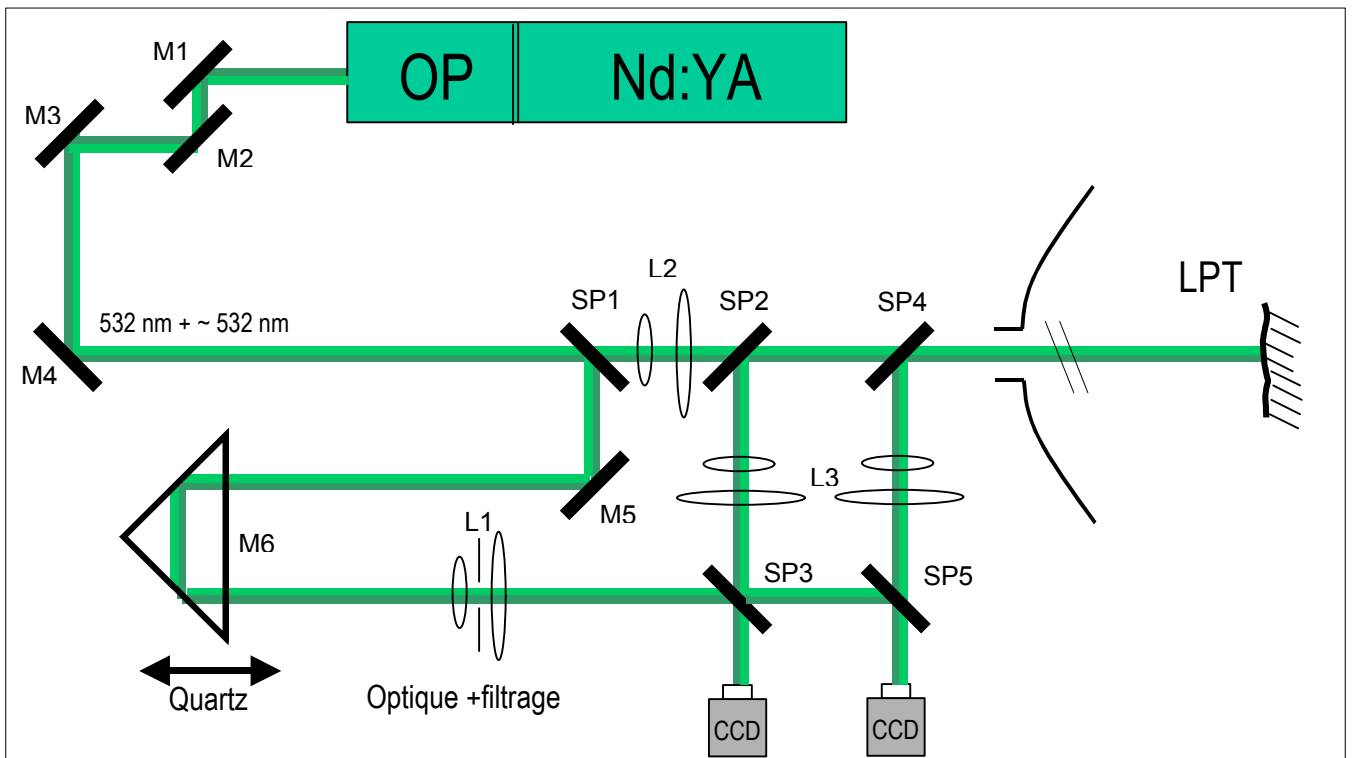


Figure 4 : Proposed design for a 2 wavelength Speckle Interferometer using an OPO laser

CONCLUSIONS

Reflection coefficient measurements have been performed on fresh and exposed tiles. Coefficient on carbon is in the range of 10 % and do not change significantly due to the redeposited layer. Two wavelengths speckle measurements have been performed by using an argon and a Yag laser. Although qualitative results have been obtained, this setting showed that it is not adequate for an erosion/redeposition diagnostic in a tokamak. Optical components but the lasers have been delivered, installed and are being used in a clean room in Cadarache. A modified design of the diagnostic based on 2 wavelengths Speckle interferometer and OPO laser has been done and further experiments are planed in a CEA laboratory to validate the proposed design.

REFERENCES

- [1] E.Gauthier et al, J. Nucl. Mater., 220-222, (1995) 506-510.
- [2] A. W. Koch, M. Ruprecht, and R. Wilhelm, "Laser Speckle Techniques for *in situ*-Monitoring of Erosion and Redeposition at Inner Walls in Large Experimental Fusion Devices," Max-Planck-Institut Für Plasmaphysik Garching bei München (1995).

REPORTS AND PUBLICATIONS

Etude de faisabilité de mesure d'ablation par interférométrie speckle à deux longueurs d'onde - G. Roupillard, E. Gauthier. CFP/CRM-2001.006.

Mesures du coefficient de réflexion du CFC dans le visible par l'Institut Fresnel (12.06.2001) - G. Roupillard, E. Gauthier CFP/CRM-2001.011.

Compte rendu de réunion au DPC à Saclay le 24 juillet 2001 - E. Gauthier CFP/CRR-2001.012.

Etude de l'érosion des composants face au plasma dans Tore Supra par interférométrie speckle - Proceedings de la conférence de la Société Française d'Optique, 21-24 nov 2001, Trégastel - G. Roupillard, E. Gauthier, V. Chalvidan.

TASK LEADER

Eric GAUTHIER

DSM/DRFC/SIPP/ICI
CEA Cadarache
13108 St Paul Lez Durance Cedex

Tél. : 33 4 42 25 42 04
Fax : 33 4 42 25 49 90

E-mail : gauthier@drfc.cad.cea.fr

Task Title: OPTIMISATION AND TESTING OPTIMISATION OF CuCrZr/SS TUBE JOINTS
Optimisation and manufacturing of samples by diffusion bonding

INTRODUCTION

During the EDA there was considerable success in constructing full-scale vertical target mock-ups. However, driven by the requirements of RTO/RC-ITER, this task aims to investigate the possibility of developing cost effective alternatives to the reference design. The objective of this task is the further development and qualification of a diffusion-bonding technique for CuCrZr to stainless steel tube to tube connection. Such junction is currently achieved using friction or welding techniques. In order to overcome drawbacks associated with Cu melting and to provide a reliable and tight joint, a diffusion-bonding technique is proposed.

In this report are described the results obtained in the optimisation of the diffusion bonding route in terms of helium leak test and tensile tests. After the optimisation of the joining process, 27 samples have been produced for further tests.

2001 ACTIVITIES

The main objective of this task has been to optimise the joining process in order to reach the best results as possible on the tensile test properties of the joint. On the base of the optimised process, 27 samples have been realized for further characterizations (erosion-corrosion, tensile test, fatigue, pressure tests) [2].

1 - OPTIMISATION OF THE JOINING PROCESS

Different configurations of devices have been tested for the optimisation of the joining process.

As displayed on figure 1, the tubes to be joined are inserted within a ring made of molybdenum. The geometry of the joint between the tubes has been investigated.

Moreover, in order to increase the normal stresses on the junction during the diffusion bonding operation, the effect of an upper load has been investigated. The device was flexible enough to test several loads with the possibility to add some ring-shapes stainless steel loads.

The joining device drawn in figure 1 can thus be simply introduced in a furnace, with no need of a container as in HIP assisted diffusion bonding.

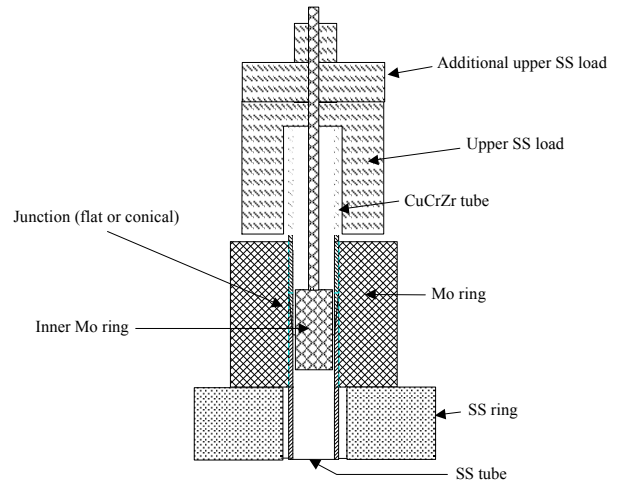


Figure 1 : Design of diffusion-bonding device

The two tubes (internal diameter: 10mm ; external diameter : 12 mm) are machined in order to have a cone-shaped, a shouldering or a flat extremity. Before connecting the tubes, the surfaces to be bonded have been carefully cleaned as follows:

- manually brushing with an alumina fibre brush and detergent,
- rinsing in a mixture of alcohol/acetone/ether in an ultrasonic bath.

To reach a sufficient load in order to impose contact between the surfaces, a Molybdenum ring is added around the tubes (diameter of the internal hole : 12.1 mm). The low value of Mo thermal expansion coefficient induces a constraint of the tubes during heating. In order to increase the normal stresses to the interface during the diffusion-bonding, an inner part made of Molybdenum has been introduced inside the tubes on one sample. To avoid diffusion bonding between the tubes and the Mo parts, a TiB layer has been deposited by spray on the rings. The tubes are placed vertically in the furnace with the 316L tube on the top. The standard thermal cycles are that described hereafter. They have been optimised in a previous study (see table 1 and [1]).

Table 1 : Tube-tube diffusion bonding parameters

Imposed Bonding T(°C)	Environment	Solutioning T(°C)	Ageing T(°C)
1025-2h-FC	Vacuum	980-2h-WQ	460-2h

FC: furnace cooling – WQ: water quenching

On the best configuration of joining (among 9 different ones), we have evaluated the dispersion of the results. For that, we have reproduced this experiment on 3 additional specimens made separately (with different thermal cycles).

The study allows evaluating the effect of the natural scattering of the process parameter on the mechanical properties of the joint. The tensile test results are displayed in figure 2.

The dispersion on the results may not hide the fact that results are relatively good as the UTS are at the same level as those obtained on the brazed junctions obtained in [1].

However, **this relatively weak reproducibility has to be explained before concluding on the suitability of this technique of joining.**

It can be seen that the behaviour of the different specimens is very different. Specimen A reaches high UTS and maximum strain while the two other ones lead to lower results. The results are also summarized in table 2.

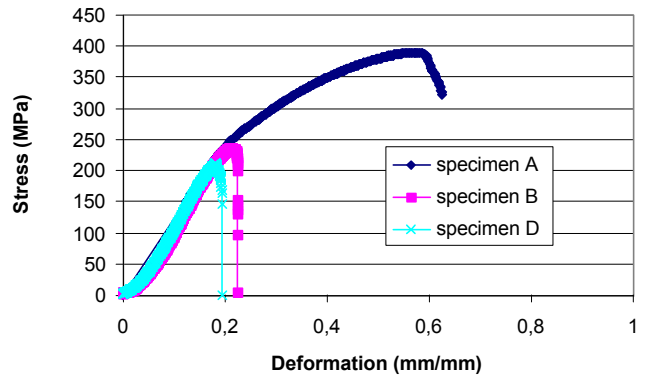


Figure 2 : Tube-tube tensile results (overall stress versus corrected displacement)


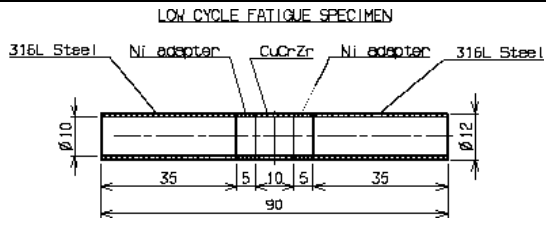

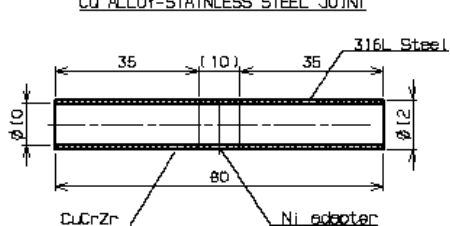

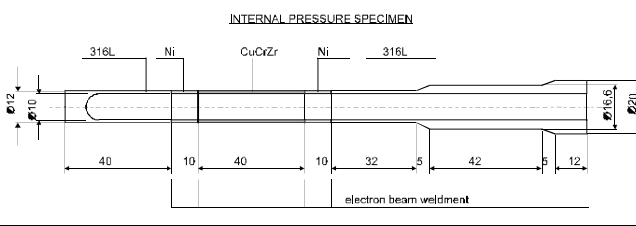
2 - MANUFACTURING OF SPECIMENS FOR FURTHER TESTS

4 x 7 additional specimens for further tests with the same configuration of joining have been realized. The tests to do and the samples geometries are indicated in table 3.

Table 2 : Tensile results on specimen A, B and D

Specimen n°	Bonding parameters	Max load (N)	Max stress (MPa)	Rupture location
A	Conical on 20 mm Tube of SS is inserted within the CuCrZr	13487	391	Failure near the junction in the Cu-Cr-Zr
B	Conical on 20 mm Tube of SS is inserted within the CuCrZr	8182	236	Failure near the junction in the Cu-Cr-Zr
D	Conical on 20 mm Tube of SS is inserted within the CuCrZr	7309	211	Failure near the junction in the Cu-Cr-Zr

Table 3 : Geometry and photos of the samples produced for further tests

Test	Samples	Drawing
Tensile test and fatigue test		<p>LOW CYCLE FATIGUE SPECIMEN</p> 
Corrosion erosion test		<p>Cu ALLOY-STAINLESS STEEL JOINT</p> 
Pressure test		<p>INTERNAL PRESSURE SPECIMEN</p> 

Specimen has been sent to external laboratories for further tests.

CONCLUSIONS

The optimisation of the diffusion-bonding route for the joining of CuCrZr/316LN tubes has been performed. The results obtained with this process are the following:

- The thermal cycle adopted was one of the best determined in [1]. It consists in a joining cycle of 1025-2h-FC under Vacuum followed by a solutioning at 980-2h-WQ and an ageing at 460-2h.

During the optimisation of the joining process on the base of the new device, it has been found that:

- the introduction of an inner ring made of Molybdenum is not necessary,
- an upper load of 1,6kg on the tube lead to the best results,
- the machining of the extremities of the tube in a cone-shape along 20 mm leads to the best results.

The results on tensile tests are correct but must be confronted to specifications before to conclude on the performances of the joining method.

In the future, an important effort must be done on the reproducibility of the results. In particular it will be necessary to explain why some of the experiments lead to relatively low UTS.

27 specimens for tensile tests, low cycle fatigue, stress corrosion and internal pressure have been manufactured and sent to external laboratories.

REPORTS AND PUBLICATIONS

- [1] L. Briottet, E. Rigal, I. Chu et B. Ricetti : EFDA TWO DV4-03 ; Optimisation of Cu-SS tube joints. Note technique DEM n° 2000/113.
- [2] L. Federzoni, P. Revirand: TVP-MAN1 Optimisation of Cu-SS tube joints, Note technique DTEN n° 2001/119.

TASK LEADER

Luc FEDERZONI

DRT/DTEN/SMP/LS2M
CEA Grenoble
17, rue des Martyrs
38054 Grenoble Cedex 9

Tél. : 33 4 38 78 57 26
Fax : 33 4 38 78 54 79

E-mail : federzoni@cea.fr

Task Title : THE JET EP DIVERTOR PROJECT

INTRODUCTION

The purpose of the enhancement is to consolidate the preparation of ITER operating scenarios, in particular with regard to ELMy H-mode operation in ITER-like configurations close to the operational boundaries and to support key ITER design choices which are still to be made. The JET enhancement proposal (under the responsibility and the supervision of EFDA CSU JET) includes an increase of the additional heating power to a level of approximately 40 MW by the addition of new NBI, ECRH and ICRH systems, and the full exploitation of these auxiliary systems necessitates an improvement in the power handling and plasma shaping capability of the JET divertor.

This project has been handed over from EFDA CSU Garching to CEA in September 2000 with the nomination of Ph. Chappuis as Project Leader. Work is done under JET orders and notifications. The European FP6 budget for fusion led the EFDA SC to give up the actual realisation of the divertor Project beginning of 2002. Nevertheless, the Design phase will be achieved nearly completely.

2001 ACTIVITIES

SCOPE

The scope of the present project is the design, research and development of the divertor including the implemented diagnostics, and the preparation of tendering documents for manufacturing of the different sub-systems. Whereas the pre-design of the divertor system has started in July 2000 as part of the JET Enhanced Performance, the design phase of the project has continued for many topics until the beginning of 2002. The procurement of all components was foreseen for 2003 which should allow to begin the assembling the divertor in 2004 in order to install the components before the end of the 2004 shutdown.

The design phase of this project has been organised in 4 main activities: Physics, Armour Tiles, Divertor Carrier & Diagnostics. The different activities were distributed in different location in Europe (Armour tile design in DEN/DM2S at Saclay, the diagnostics in foreign European associations {ENEA, FZJ, IPP, IST}, the remaining and the coordination within the DRFC at Cadarache)

DESIGN

The JET divertor is fixed on a rigid structure on the lower part of the Vessel. It has general W shape to managed the two divertor legs with two pumping throats in the bottom corners. Carbon Fiber Composite (CFC) tiles are used as the plasma facing armour.

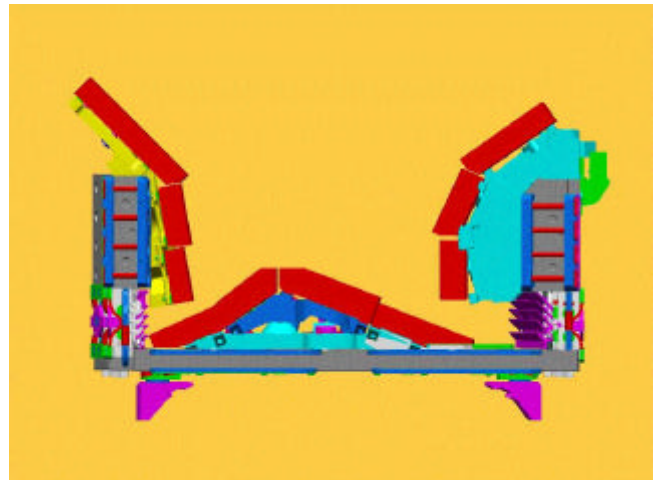


Figure 1 : MKII HP divertor concept

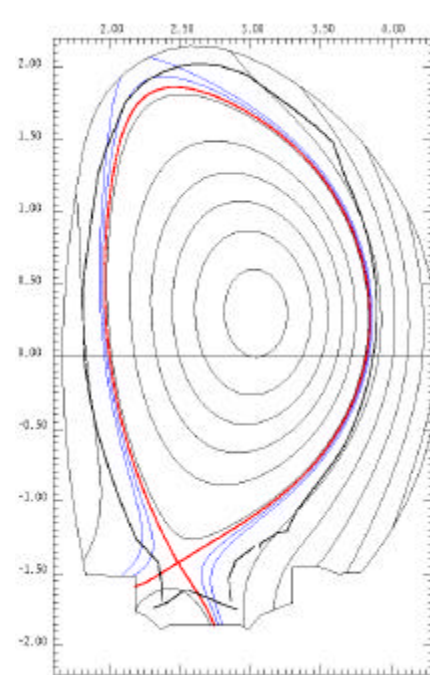


Figure 2 : High triangularity magnetic equilibria

The divertor profile (figure 1) has been adapted to match 18 reference equilibria with a prioritisation on high triangularity (figure 2) or advanced tokamak scenarios.

The profile of each tiles has been designed to shadow every edges in all 18 scenarios (figure 3).

The thermal and mechanical behaviour of the tile and attachment system were simulated for the priority scenario and the poloidal profile (figure 4) was optimised to sustain the 28 MW of incoming power with a surface temperature less than 1800°C.

The tile material and the machining were fully specified.

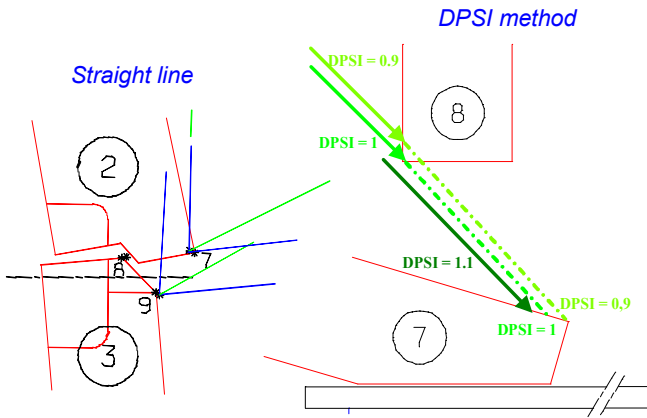


Figure 3 : 2D analysis of poloidal shadowing

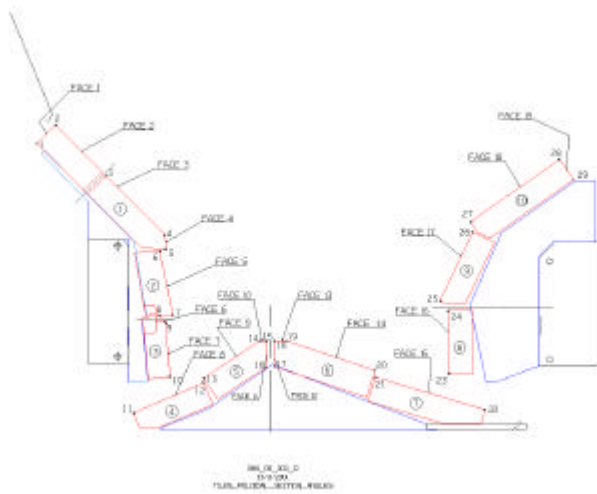


Figure 4 : 2D poloidal profile of the divertor

The carriers were designed to support the tile in position during electro dynamical efforts (halo & eddy current), to interface the divertor with the vessel and to integrate the relevant diagnostics (figure 5). Specific features were adapted to allow the divertor to be remote handleable

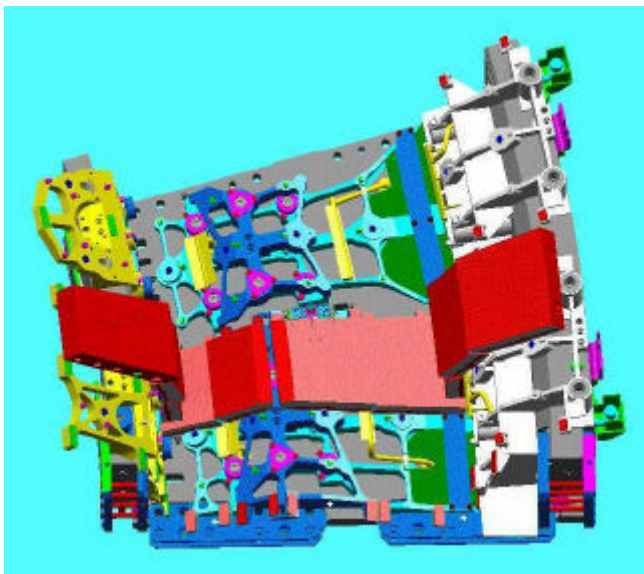


Figure 5 : Catia model of the divertor elements (issue Sept. 2001)

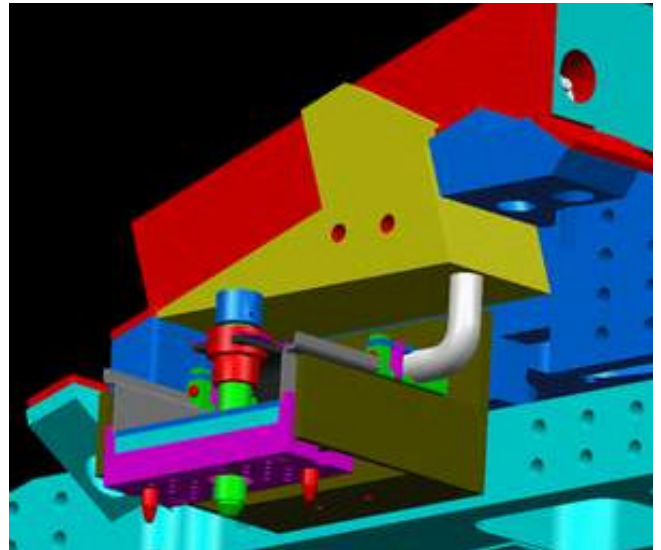


Figure 6 : Diagnostic envelope for a pressure gage

Based on the MK II A & MK II GB experience, diagnostics envelopes were defined and the interfaces to carrier and tiles were fixed in order to allow an autonomy of the associations for the design.

DEVELOPMENTS

High heat flux thermomechanical tests were performed on a new thick CFC material (200 mm perpendicular to fibre planes) in the Jet NBI test bed. The material showed similar performance to the one in use on the previous divertors.

Carrier fast prototypes were manufactured (figure 7) to prepare the diagnostics cabling routes, the casting procedure and the assembling of the divertor.

To sustain the high mechanical loads in the carriers at high temperature, requires the use of an Inconel material.

To reduce the manufacturing delays, a vacuum cast solution followed by a HIPed cycle was proposed and validated trough mock-ups (figure 8) and characterizations.

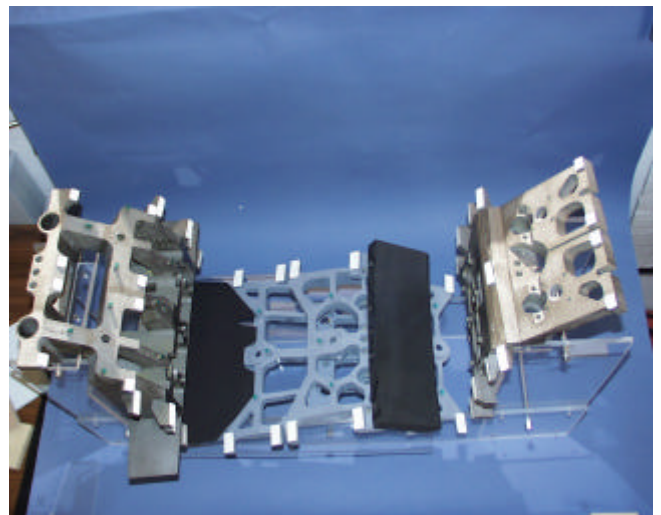


Figure 7 : Prototyping of the divertor elements (issue Nov. 2001)



Figure 8 : Carrier mock up Inconel 650 vacuum cast & Hipped

TASK LEADER

Ph. CHAPPUIS

DSM/DRFC
CEA Cadarache
13108 St Paul Lez Durance Cedex

Tél. : 33 4 42 25 46 62
Fax : 33 4 42 25 49 90

E-mail : pchappuis@cea.fr

DELIVERABLES

In 2001 the divertor design was achieved and reported in design reviews at JET.

The majority of the divertor drawings were completed.

The technical specifications were written.

The project design phase should be fully (except some diagnostics) achieved in 2002.

UT-PFC&C-HIP

Task Title : MECHANICAL BEHAVIOUR OF HIP JOINTS

INTRODUCTION

The main objective of this task is to characterise the mechanical behaviour of joints fabricated using the Hot Isostatic Pressing (HIP) process, which is currently one promising joining technique [1]. Both HIP 316LN to 316LN, and 316LN to a precipitation strengthened alloy (CuCrZr) joints will be tested. Previously, a programme on an oxide dispersion strengthened Cu alloy (Cu-Al-25) was conducted [B. MARINI, 1998]. Copper alloys are candidates for heat sink as first wall, divertor, limiter, baffle components. Validation of fabrication techniques requires performing mechanical properties such as impact test resistance (Charpy U), toughness, fatigue and thermal fatigue. The aim of the thermal fatigue programme is to get a better knowledge of component behaviour under severe cyclic peak temperature representative of in-service conditions.

All tested HIP joints were manufactured by the Tecphy society. The selected fabrication conditions were respectively 1100 °C, 140 MPa, 2 hours for 316LN to 316LN joints and 920 °C, 100 MPa for 316LN to CuCrZr. A first 316LN to 316LN HIP joint lot was rejected for unacceptable impact test resistance results. A second 316LN to 316LN HIP joint fabrication has been accepted. Both ultrasounds and dye penetrant tests do not show any major defect. All the tests on this lot are now completed.

2001 ACTIVITIES

Test programme is ended since 2000. Results are presented in a final report (NT SRMA 02-2480).

MAIN RESULTS AND CONCLUSIONS

The new 316LN to 316 LN HIP joint has a good mechanical behaviour. These results are plainly confirmed by all the mechanical tests such as tensile, toughness, four points bending tests.

Under tensile loading, necking at rupture is about 50 % (figure 1). Scattering behaviour on the joint shows that very accurate fabrication conditions are needed.

Good quality is plainly underlined by the four points bending tests. Final rupture can occur out of the diffusion-bounding zone (figure 2).

CT 20 specimen testing confirmed plainly the good behaviour of the 316 LN/ 316 LN HIP joint. Jr-Da curve is presented on figure 3.

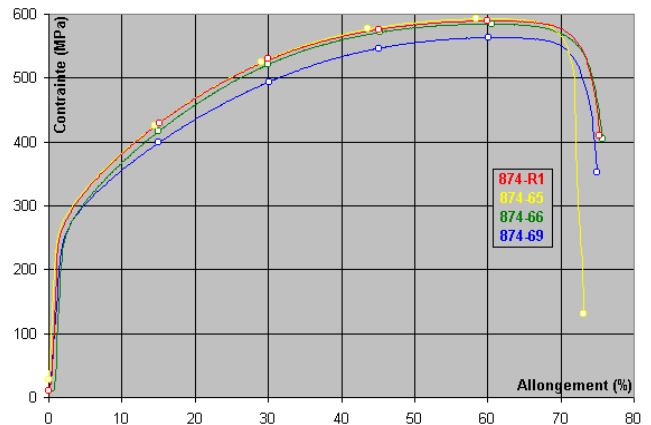


Figure 1 : Plate specimen tensile tests 2nd fabrication. Stress as a function of strain

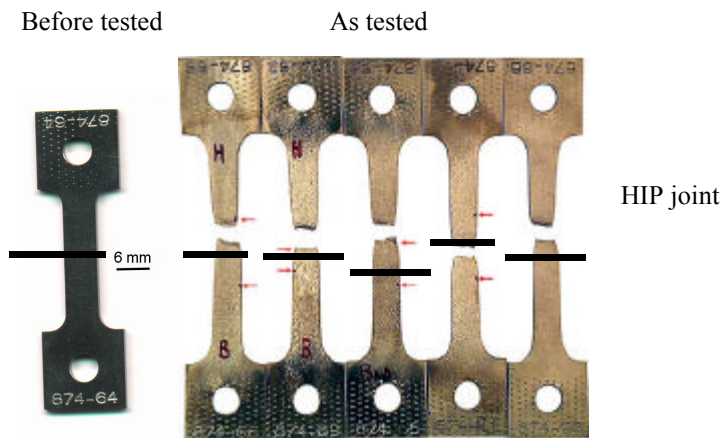


Figure 2 : Plate specimen tensile tests (HIP bounded-zone corresponds to the full line) 2nd fabrication. Specimens before and after test.

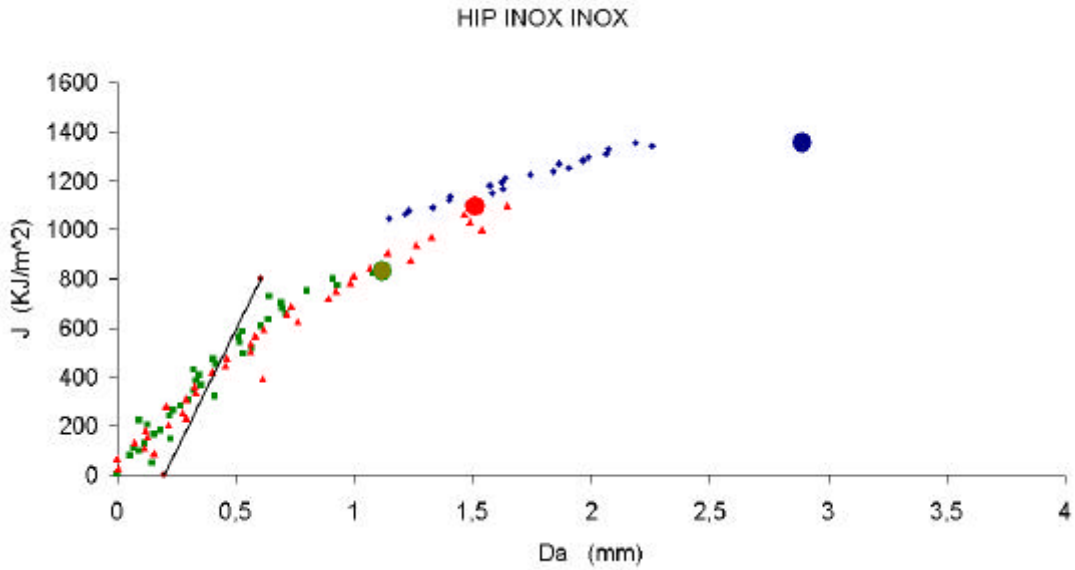


Figure 3 : Toughness properties of the 316LN to 316 LN HIP joint 2nd fabrication
Jr – Da curves obtained with CT 20 specimen testing, full symbols correspond to post-mortem measurements.

Crack growth resistance has been determined using CT20 specimens.

Concerning Copper/ 316 LN joint, crack initiation corresponds approximatively to 10 - 20 MPa m^{0.5} (figure 4). Such values appear to be very low.

But all are nevertheless significantly higher than one previously measured on Glidcop 316 L joint [2] to [4].

As it is confirmed by the thermal fatigue test programme, 316 LN copper joint is acceptable.

No crack was detected using ultra-sound control [5] up to 50 000 cycles for measured surface temperature range fixed to 70 °C (figures 5 and 6).

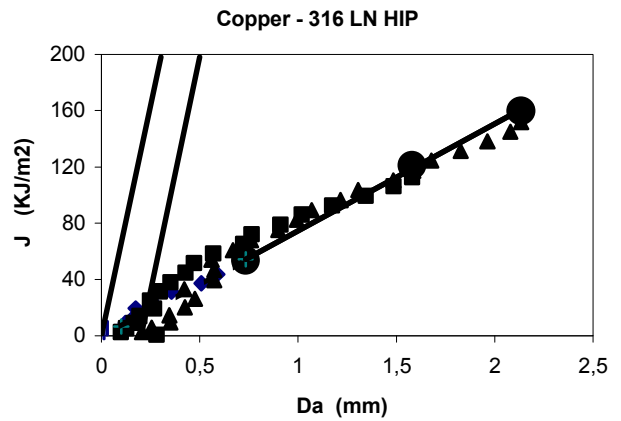


Figure 4 : Jr - Da curve for the copper to 316 LN joint,
full symbols correspond to post mortem measurements

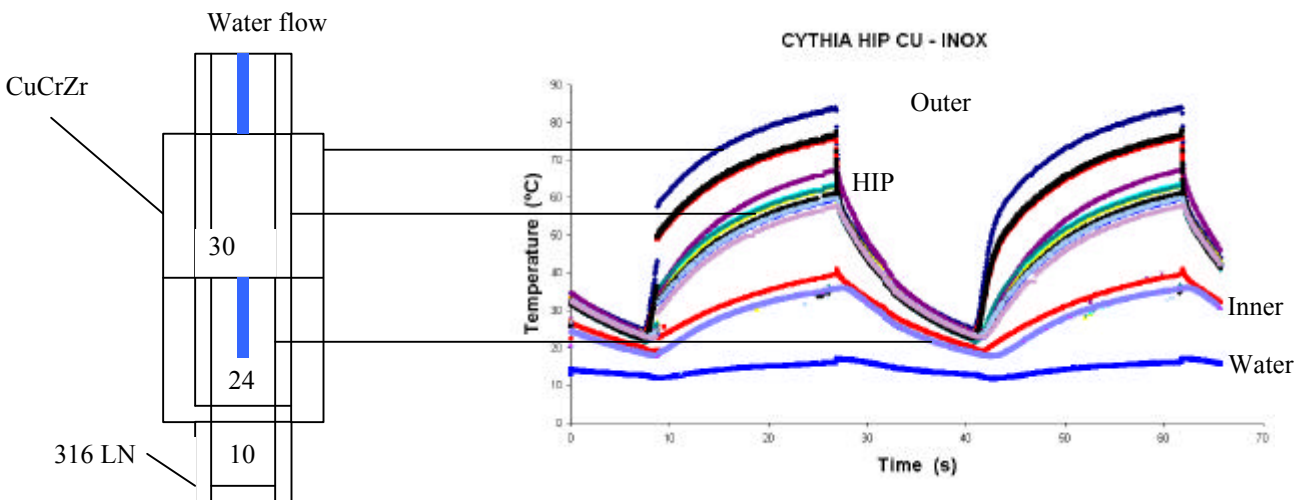


Figure 5 : Temperatures as a function of time determined on reference specimen.
Thermocouples are placed in different zones

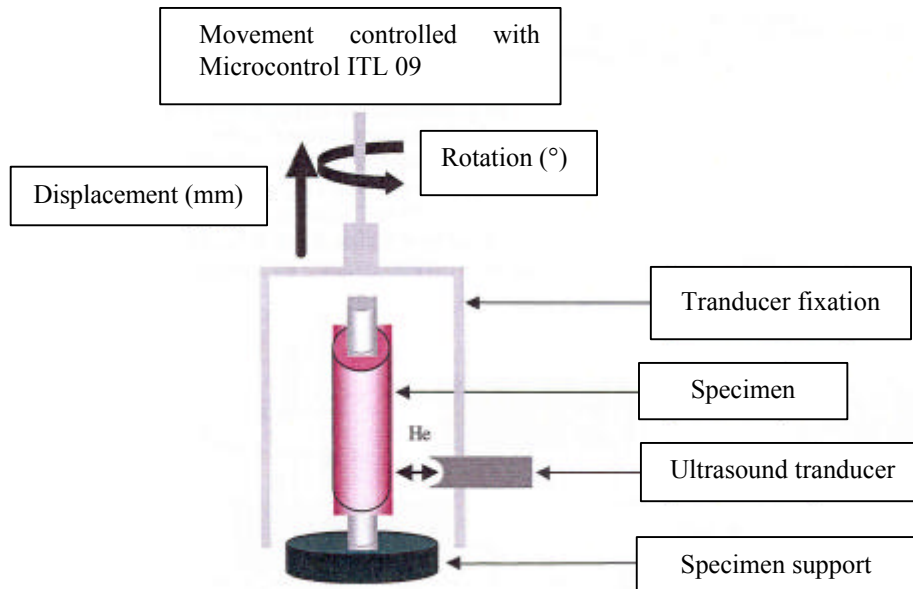


Figure 6 : Ultrasound control methodology used for the Copper/ 316 LN HIP joints before and after thermal fatigue test on the CYTHIA facility

REFERENCES

- [1] A. A. TAVASSOLI, ISFNT, presented at Tokyo (Japan), April 6 – 11, 1997.
- [2] P. FORGET, P. WIDENT, Compte Rendu SRMA 98 – 1600.
- [3] J.M. GENTZBITTEL, G. NOMBALAI, B. RICETTI, H. BURLET, Note Technique DEM/ CEA 97 – 66.
- [4] B. MARINI, 1998, Final Report ITER T214, Subtask CEA - 9, CEA - 10, CEA – 11, NT SRMA 98 – 2278.
- [5] J. GODEFROIT, Note DECS/STA/LMUS/01-RT4012/Rév.0.

TASK LEADER

A. FISSOLO

DEN/SAC/DMN/SRMA
CEA Saclay
91191 Gif-sur-Yvette Cedex

Tél. : 33 1 69 08 31 02

E-mail : antoine.fissolo@cea.fr

REPORT

A. FISSOLO - Mechanical behaviour of HIP joints - NT SRMA 02-2480.

Task Title : BORON DOPED GRAPHITES

INTRODUCTION

Owing to its low atomic number, good mechanical and thermal properties, graphite is an attractive candidate as protection material for the first walls of fusion reactors. Previous studies showed that the addition of boron to graphite improves the erosion behaviour. The objective of the present work was to investigate the effect of atomic boron addition on the relevant graphite properties.

Thus, B-doped, highly dense materials were prepared using powder technology techniques, i.e. powders mixing, cold isostatic pressing (CIP), and hot isostatic pressing (HIP) which are well under control at CEA. Thermal and mechanical properties of the boron/graphite composites were characterized.

2001 ACTIVITIES

Three boron/graphite composites containing 10, 20 et 30 % vol. of boron were elaborated following both process and parameters definite in 2000.

After mixing powders in a jar and ball milling, different compositions C/B were shaped by cold isostatic pressing technique and densified by hot isostatic pressing technique at 1600°C – 190 MPa.

The following characterizations were performed on the sintered materials:

- density
- Vickers hardness
- thermal conductivity
- Bending test
- Young's modulus

DENSITY

The density was measured by immersion in liquid on the samples sintered at 1600°C – 190 MPa. If we suppose that the reaction between graphite and boron is total during the heat treatment ($C+4B \rightarrow B_4C$), we get the results summarized in table 1.

VICKERS HARDNESS

Measurements of the Vickers hardness were performed using a micro hardness tester LEICA VMHT 30A. For each sample, the measurement was repeated 10 times under a load of 50 grams for 15 seconds. The results are shown in table 2.

Table 1 : Density of composite Bore/Graphite densified by HIP, with total reaction $C+B \rightarrow B_4C$

Ref.	XIX 145	XIX 146	XIX 147
Bore (%)	10	20	30
D (theo) g/cm ³	2,30	2,33	2,36
D (hydro) g/cm ³	2,23	2,24	2,23
Open porosity %	0,03	0,00	0,00
Closed porosity %	3.03	3.95	5.60
Total porosity %	3.06	3.95	5.60

Table 2 : Vickers Hardness (50 g) of composite Bore/Graphite densified by HIP

Ref.	XIX 145	XIX 146	XIX 147
Bore (%)	10	20	30
Hv _{50g} moyen	3.8	3.9	4.7
Ecart type	0.2	0.6	0.3

The hardness increases with the content of boron in the composite. From 10 to 30 % of boron the hardness increases of 20 %.

THERMAL CONDUCTIVITY

The thermal conductivity is estimated by the product of the density by thermal diffusivity by specific heat capacity. Thermal diffusivity and specific heat capacity measurements have been presented in previous report [1]. The density is corrected from the thermal expansion. No measurement was done and the value retained was the coefficient of linear thermal expansion of $5.10^{-6} K^{-1}$.

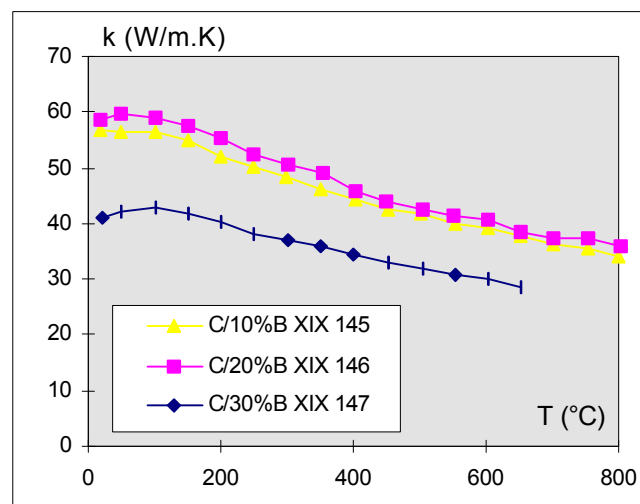


Figure 1 : Thermal conductivity of B/C composites

The accuracy is of the order of $\pm 8\%$ in absolute value, but of the order of $\pm 4\%$ between the curves (mistakes due to identical Cp). The conductivities of the materials containing 10% and 20% of boron are almost the same (figure 1) despite the differences of the relative densities and of the microstructures (shape of the porosities). Globally thermal conductivity of B/C composites decreases with the content of boron.

3 POINTS BENDING TEST

The tests of 3 points bending were obtained using a 40505 INSTRON machine. The measurements at room temperature have been made with a length of 40 mm between support.

For each composite, 7 tests bars (4 x 4 x 45 mm) were tested. Samples were beveled and ground-in. The modulus of rupture is obviously the same for the materials containing 10% and 20% of boron. Best results are obtained with the 30 vol% boron composite (figure 2).

YOUNG'S MODULUS

The measurements of Young's modulus were performed at the Société Française de Céramiques by the vibratory method on test bars 4 x 4 x 50 to 70 mm. Young's modulus values of B/C composites are directly bounded with the content of boron in materials.

Young's modulus increases almost linearly with the content of boron (figure 2)

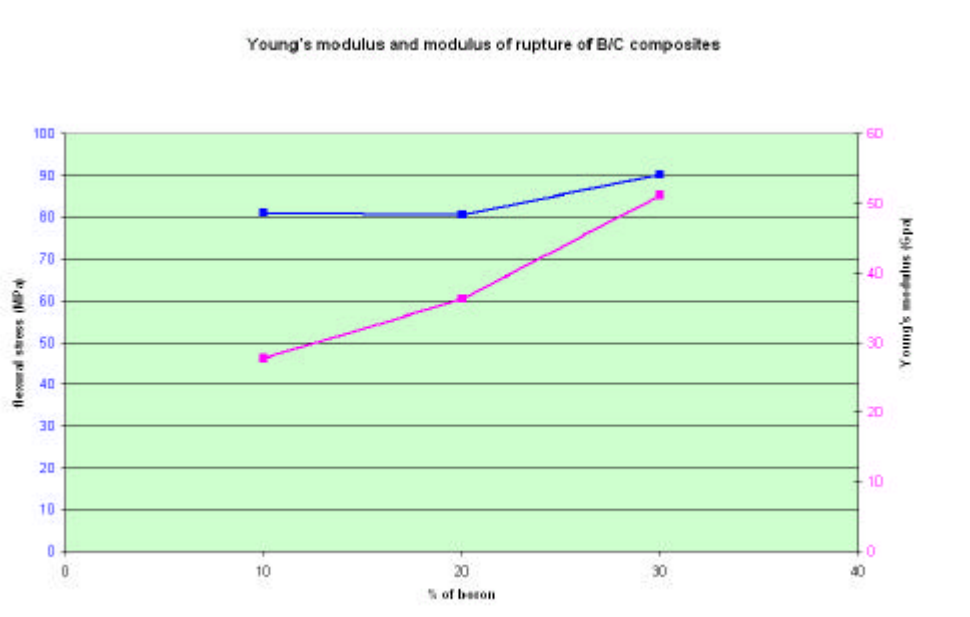


Figure 2 : Young's modulus and modulus of rupture of B/C composites in bending test

CONCLUSION

The objective of this work was to investigate the effect of atomic boron addition on the graphite properties. We have shown that a homogeneous structure can be obtained by mixing powders in jar and ball milling. Composites made of graphite with different boron content, from 10 to 30 vol% were elaborated. Density measurement performed on various samples with different boron content showed that boron eases densification. After HIP treatment at 1600°C – 190 MPa, porosity is closed and reaches about 3-5%. The characterizations realized on dense B/C composites showed that boron addition increases hardness, Young's modulus and modulus of rupture. On the other hand boron insertion is detrimental to the B/C composite thermal conductivity.

REFERENCES

- [1] N.Lochet. Boron – doped graphites. Mechanical and thermal characterization, January – June 2001 report CEA/DRT/DECS/SE2M/LECMA 01-DT-14 - 27/06/2001.

REPORTS AND PUBLICATIONS

N.Lochet. Boron – doped graphites. Mechanical and thermal characterization, January – June 2001 report CEA/DRT/DECS/SE2M/LECMA 01-DT-14 - 27/06/2001.

N.Lochet. Boron – doped graphites. Mechanical and thermal characterization, Final report CEA/DRT/DECS/SE2M/LECMA 01-DT-26 – 15/11/2001.

TASK LEADER

Nicolas LOCHET

DRT/DECS/SE2M/LECMA
CEA Saclay
91191 Gif-sur-Yvette Cedex

Tél. : 33 1 69 08 32 16
Fax : 33 1 69 08 57 54

E-mail : nicolas.lochet@cea.fr

Task Title : DEVELOPMENT OF SiC/METAL JOINING TECHNIQUES

INTRODUCTION

The aim of the task is to perform mechanical tests and characterize the junction between ceramic and metal. Indeed such duplex structures, especially assemblies of composite SiC_p/SiC and tungsten components, are attractive for the elaboration of plasma-facing armor material according to the current design of Tokamak divertors.

2001 ACTIVITIES

Several sets of SiC/W assemblies have been elaborated to perform mechanical testing at room temperature and at 800°C. Ceramic and metal parts have been brazed with the Brasic® H1 process. The brazing temperature is quite high 1530°C. Due to the differences in the thermal expansion of the materials, significant residual stresses are created in the structure during the cooling down.

The sandwich-like structure is illustrated by the figure 1. Specific mounting device has been used to obtain good alignment and parallelism during the brazing operation [1].

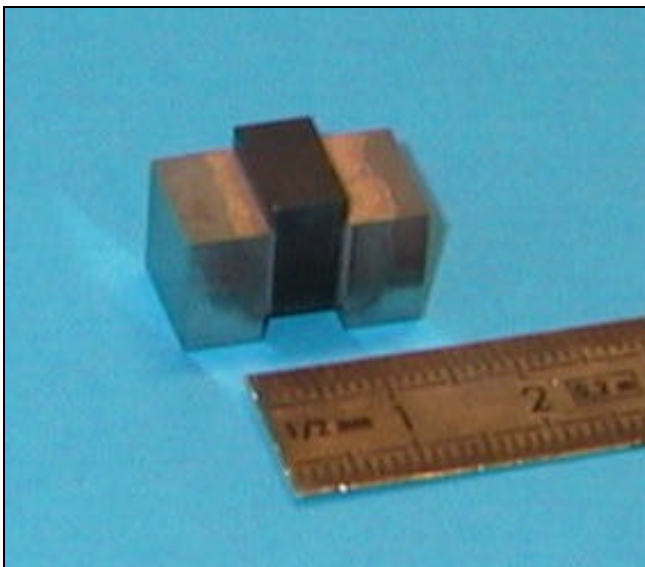


Figure 1 : View of a mechanical test sample W/SiC/W

Mechanical tests have been performed by applying an axial load on the central part of the structure.

The mean shear strength was evaluated to be 6,5 +/- 2 MPa at R.T and 8,5 +/- 1,1 MPa at 800°C. All the ruptures occurred in the brazing layer.

The figure 2 shows a typical displacement vs. axial force recorded during the mechanical test.

Interpretation of these experimental results is quite difficult because the loading of the structure is the combination of residual and test-induced stress fields.

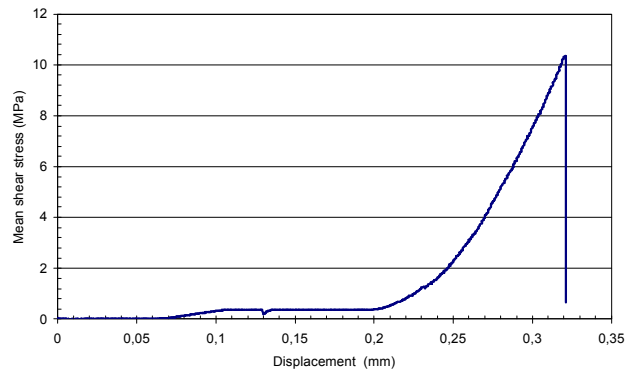


Figure 2 : Displacement vs. force curve recorded during mechanical loading of a SiC/W/SiC structure

Finite Element analysis (CASTEM 2000) has been carried out in order to determine which parts of the structure are submitted to the maximal stresses and what kind of solicitation is locally applied. In a first approach, residual stresses are not modeled in order to evaluate only the magnitude of the mechanical loading. This calculation gives some elements for the interpretation of experimental results and allows a critical analysis of the test :

- It has been shown that the loading along the interfaces is the combination of two main modes : shear and flexion, and also axial compression. The lower part of the junction is solicited in traction and shear, whereas the upper part is in compression as a consequence of the bending. In the upper region of the interface, the stress concentration is important : As illustrated by the figure 3, the Von Mises equivalent stress is five times higher than the mean value of shear stress.
- Thus, the strengths of assemblies evaluated on the assumption of a pure shear loading have to be re-evaluated in order to take into account the bending components. Some improvement of the test design has been suggested in order to promote one mode of loading (bending vs. shear for instance).
- The stresses values induced by a mechanical loading which corresponds to the experimental conditions of rupture and calculated in the structure are quite low (50 MPa, excepting in the vicinity of the inner corners because of the non-representative geometrical singularities).

Secondly, the residual stresses induced by the mismatch of physical and mechanical properties of materials during the cooling down have been simulated.

It was stated that the residual stresses in the structures reaches 150-200 MPa in the base material SiC and W.

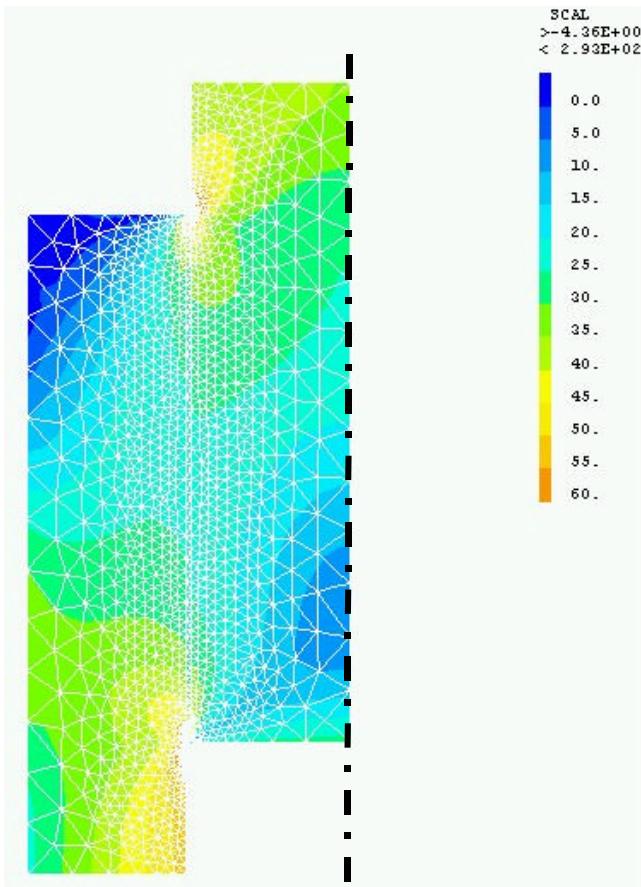


Figure 3 : Map of Von Mises stresses during loading of a sandwich-like structure (half-part is represented) at 40 MPa applied on the upper face and without consideration of thermal stresses (mean shear in the junction is 12 MPa that corresponds to the maximal exp. value of shear strength)

In fact, the mechanical behaviour of the brazing layer itself has an influence on the residual stresses repartition as illustrated by the figure 4. In this calculation the ductile behaviour above 800 °C of the brazing alloy has been taken into account for the simulation of the cooling down after brazing.

This analysis has also demonstrated that the main residual stress are localized inside the brazing layer due to the strong differences of the thermal expansion of the brazing alloy and base material (SiC and W).

The junction has also been characterized by Scanning Electron Microscopy and the reactivity previously observed between brazing alloy H1 and W, has been analyzed. It was pointed out that several binary and ternary phases constitutes the reactive zone. Large pores are also observed in the interface (figure 5).

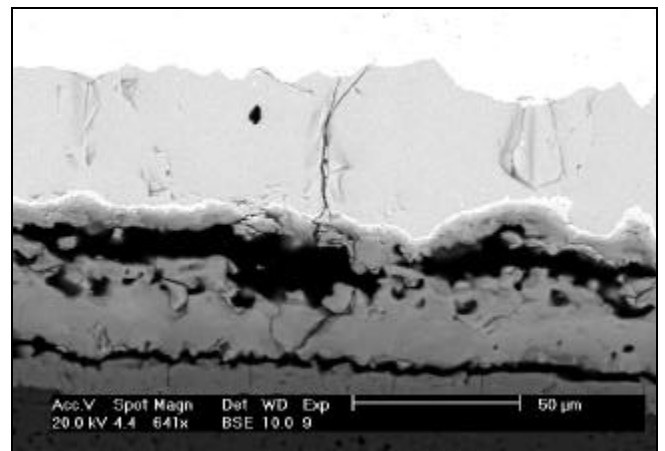


Figure 5 : Observation of SiC/W junction by SEM. The reactive layer (grey) between brazing alloy (down, dark) and W (up, white) and also pores can be observed

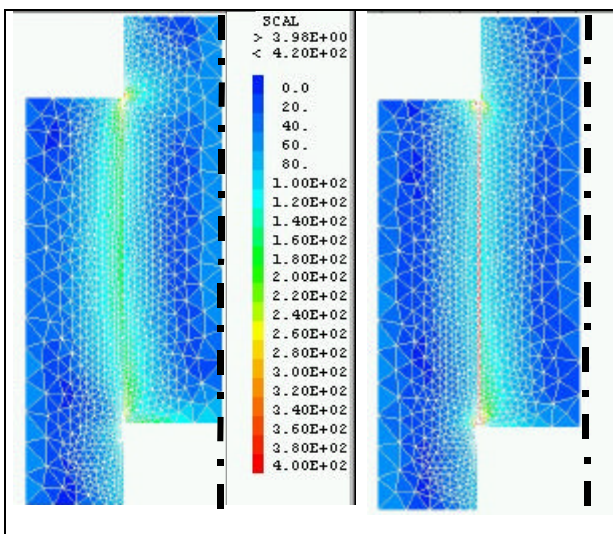


Figure 4 : Map of Von Mises stresses after cooling down of a SiC/W/SiC structure (half-part is represented) without (left) and with consideration (right) of the mechanical behaviour of the brazing layer

A mechanism for the formation of this porosity has been proposed. The evolution of chemical composition of the brazing alloy due to reactivity with W would lead to a partial solidification and creates volumetric restraint at the brazing temperature.

As a consequence, it is concluded that the brazing layer is the weakest part of the tested SiC/W structures [2].

CONCLUSIONS

1. Sandwich-like structures (SiC/W/SiC or W/SiC/W) of brazed material can be elaborated with tailored geometry and good parallelism in order to perform mechanical tests at room temperature and at 800°C. The shape of the samples, which is not the standard geometry for the evaluation of shear or bending stresses, takes into account the limitations brought by the use of composite materials.

2. The stress distribution in the structure is quite complex and is the combination of thermal residual stresses and mechanical loading. For the evaluation of residual stresses, the thermo-mechanical behaviour of the brazing layer has to be taken into account. In the case of Brasic® H1, the plasticity of the alloy above 800°C and its brittle behaviour at room temperature accommodates the thermal expansion mismatch during cooling down.
3. The mechanical loading creates both shear and tension at the interface of base materials and also induces stresses concentration due to the geometry of the structure. We stated that the local stress level can be five times greater than the mean stress. Finally, for the SiC/W structures tested in 2001, the levels of stresses induced by the loading are much lower than the thermal residual stresses. All these points lead to some severe restriction to use directly the experimental strength in a dimensioning purpose.
4. The design of the test should be modified to aim at limiting the weight of thermal stress in one hand and at promoting one mode of loading on the other. These improvements would allow to interpret more precisely the intrinsic strength of the junction. Furthermore, experimental data have to be analyzed with the Weibull statistics in order to obtain dimensioning results. This approach implies that a significant amount of tests would be performed.
5. The reactivity of the braze alloy with tungsten is a limiting factor for the junction strength. Indeed, the presence of large pores in the reactive layer likely constitutes initiation sites from where cracks can propagate at low temperature during loading. The brazing process may be improved either by the use of a less reactive braze alloy (which would have also a more compatible thermal expansion coefficient) and/or by a better junction design including interfacial layers. Nevertheless, the mean strength obtained with Brasic® H1 at room temperature (6,5 MPa) is close to values reported in other studies where SiC/metal junction has been tested. Finally, the resistance at high temperature (>800°C) is expected to be greater due to the ductile behaviour of the brazing layer and the decrease in the residual thermal stresses.

REPORTS AND PUBLICATIONS

- [1] F. SAINT-ANTONIN. UT-PFC&C-SiC/MJ, Development of SiC/metal joining technology, complement to the 2nd progress report. Note Technique DTEN n°121/2001.
- [2] G. DELETTE. UT-PFC&C-SiC/MJ, Development of SiC/metal joining technology, 3rd progress report. Note Technique DTEN n°25/2002.

TASK LEADER

Gérard DELETTE

DRT/DTEN/SMP/LS2M
CEA Grenoble
17, rue des Martyrs
38054 Grenoble Cedex 9

Tél. : 33 4 38 78 38 53
Fax : 33 4 38 78 54 79

E-mail : gerard.delette@cea.fr

UT-VIV/PFC-W/COAT

Task Title : DEVELOPMENT OF THICK W CVD COATINGS FOR DIVERTOR HIGH HEAT FLUX COMPONENTS

INTRODUCTION

The main objective of this study is demonstrate the feasibility of thick tungsten deposition on copper alloy used for divertor high heat flux components.

Bibliographic study has demonstrated that WF_6/H_2 chemistry would be the most interesting chemistry for our first investigation because of the high level of knowledge of this chemistry and easy to put in place on a pilot CVD reactor. In addition thermodynamic has shown that we can keep the chemical integrity of the copper substrate by using this chemistry.

First tungsten CVD coating on copper substrate have been successfully performed on a pilot CVD reactor. Process results has shown a good agreement with literature knowledge. Preliminary study on mechanical properties of the tungsten coating has shown the excellent adhesion of film up to 60 μm .

2001 ACTIVITIES

A literature review was performed to revue tungsten precursors for chemical vapor deposition. Both metal organic^(1,2) and halides^(3,4) precursors have been listed. Halide chemistry like tungsten hexafluoride has shown is superior robustness mainly because this precursor is the most well known in CVD tungsten coating technology. The process conditions for such chemistry requires a mass control regime in order to minimize intrinsic stresses. Only main concern is the potential high reactivity of fluorine precursor on copper substrate.

Thermodynamic calculations on the (Cu-W-F-H) system were carried out in order to check the compatibility of chemical vapor deposition from tungsten hexafluoride on copper substrate. This approach gives the equilibrium conditions of the studied system as a consequence allows to obtain higher level of calculated values. This approach is based on restrictive hypotheses.

The first assume that the thermodynamics balance is reached, what is justified when the temperature, the pressure in the reactor, or the species waiting time are high.

The second assume that the reactor where take place reactions is a closed system. The conditions of calculations are typical CVD process conditions.

Temperature is in the range of 400 K (127°C) and 1000K (727°C), total pressure is the range of 10^{-4} atm (approximately 0,1 Torr) and 1 atm. WF_6 's dilution of 1 % in H_2 will be consider. The copper substrate will be taken into account as some copper in excess, that means 10 moles of copper.

All species taken into account in the thermodynamics calculations is given in the following table:

Table 1 : Species taken into account for thermodynamic calculation

Solid species	Cu	CuF	CuF ₂	WF ₄	WF ₅
	WF ₆	W			
Gas species	Cu	Cu ₂	CuF	CuF ₂	Cu ₂ F ₂
	Cu ₃ F ₃	CuH	F	F ₂	HF
	F ₂ H ₂	F ₃ H ₃	F ₄ H ₄	F ₅ H ₅	F ₆ H ₆
	F ₇ H ₇	WF	WF ₂	WF ₃	WF ₄
	WF ₅	WF ₆	H	H ₂	W

In the ranges of temperature [400K - 1000K] and total pressure [10^{-4} atm-1 atm], the reaction of a gas mixture consisted of 1 % of WF_6 in H_2 on some copper give place to a tungsten deposition with 100 % yield. The WF_6 precursor is fully decomposed in solid tungsten.

Gas products are mainly H_2 (vector and reducing gas), HF, H_2F_2 , H and in very small proportions (with molar fractions less than 10^{-8}) copper based gas compounds like, CuF, CuH, Cu.

Figures 1a and 1b give respectively the influence of temperature (at 10^{-2} atm) and pressure (at 773 K) on products and their molar fraction formed at the balance.

These figures show that there is an increase of copper attack by the gas mixture when the pressure decrease and the temperature increase.

However, the molar fraction of copper base species in the gas phase is in the order of 10^{-13} , what suggest a negligible degradation of the copper substrate.

First sets of experiments were performed in order to validate the potential of tungsten hexafluoride precursors for tungsten coating on copper substrate with a thickness up to 10 μm . A low pressure hot wall reactor has been used with a process temperature and pressure respectively at 773 K (500°C) and 38 mbar.

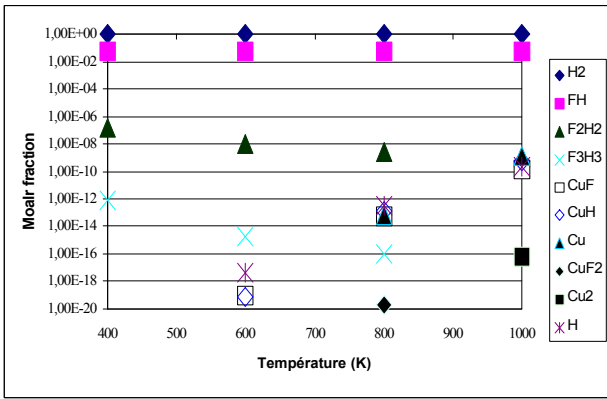


Figure 1a : Influence of temperature on molar fraction of products at 10^{-2} atm or approximately 10 Torr

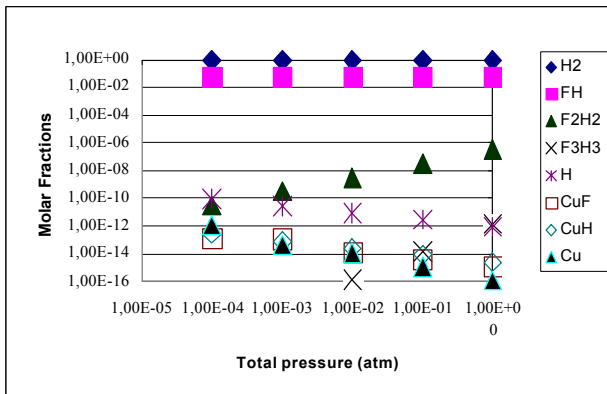


Figure 1b : Influence of total pressure on molar fraction of products at 773 K or 500°C

Figure 1 : Molar fractions of gas products at the balance from the reaction $\langle \text{Cu} \rangle + \text{WF}_6 + \text{H}_2$.
Conditions of calculations: $\langle \text{Cu} \rangle = 10$ moles;
 $x_{\text{H}_2} = 0.99$, $x_{\text{WF}_6} = 0.01$

Kinetics has been estimated by varying thickness with deposition time as shown in figure 2.

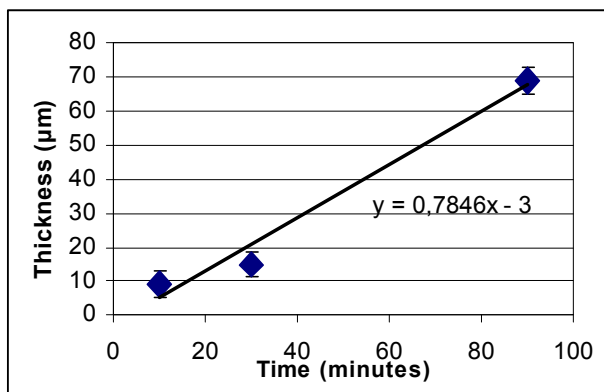


Figure 2 : Thickness versus deposition time for tungsten film deposited at 500°C, 38mbar, and with WF_6/H_2 respectively at 80/1000 sccm

Process conditions give a 0.78 $\mu\text{m}/\text{min}$ deposition rate with an incubation time approximately of 4 minutes. This incubation time is below our measurement precision.

However it is possible that our sample preparation cannot completely remove hydrocarbon at the copper surface which enhance incubation time for tungsten growth. We can noticed that tungsten film with 69 μm thickness has been deposited.

SEM view and XRD scans show a very rough and highly textured ((200) oriented) coating as shown respectively on figure 3 and 4.

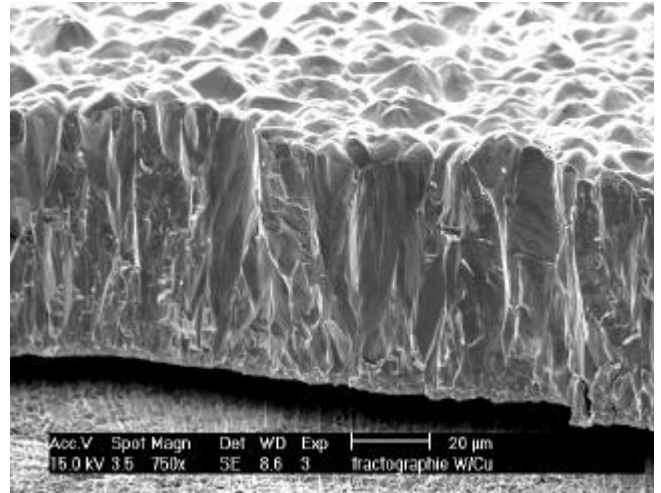


Figure 3 : Oblique SEM view of a fractured cross section of the 69 μm tungsten film. Growth conditions are: Deposition time: 90 minutes, temperature : 500°C, Pressure: 38 mbar, WF_6/H_2 flow: 80/1000 sccm

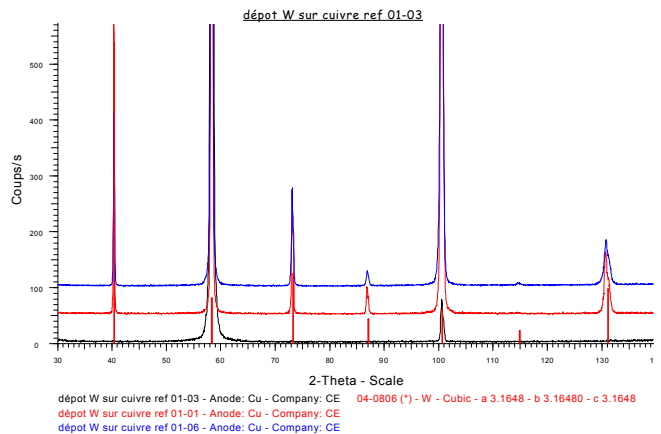


Figure 4 : Tungsten XRD scans for three different deposition time: Blue: Deposition time: 10 minutes; Red: deposition time 30 minutes, Black deposition time 90 minutes. Process conditions are the same for all coatings: pressure: 38 mbar, Temperature: 500°C, H_2/WF_6 : 1000/80 sccm

The influences of interface design on film adhesion were evaluated by scratch tests. Meanwhile, the critical load, L_c , which indicates adhesion strength, is determined by the onset of a sudden variation in friction forces as a diamond stylus scratching tungsten films.

L_c is correlate with an optical inspection of the scratch track. Table 2 summarize the critical load, L_c as a function of the tungsten thickness.

Table 2 : Adhesion strength of tungsten coating as a function of film thickness

Tungsten thickness (μm)	Critical load (Newton)
9	25
15	70
69	100

Results from table 2 show that lower thickness almost delaminates right off the substrate surface during testing while, the thicker film show a very good adhesion strength. This behaviour could be attributed to a relaxation of internal stress in the film when film thickness is higher. Further investigation will be performed in order to understand the mechanism of this behaviour.

CONCLUSIONS

The first stage of this work has demonstrated the feasibility of such technology. Thermodynamical analysis and preliminary tungsten deposition on copper substrate were performed this year. We have shown that tungsten hexafluoride and hydrogen chemistry used for tungsten deposition has no effect on the integrity of the copper substrate and the tungsten coating with a maximum tungsten thickness up to 60 μm .

This feasibility study has allowed us to define a path for our further investigations.

The research regarding tungsten coating will focus on:

- Finding the optimal process parameters for tungsten thicknesses up to 100 μm .
- Determining the internal residual stresses in the coating as a function of the process parameters.
- Finding optimal thermomechanical properties of tungsten coatings.
- Eventually developing suitable inter layers to improve the bonding and other mechanical properties.

REFERENCES

- [1] L.H. Kaplan, F.M. D'Heurle, J. Electrochem.Soc. 117 (1970) 693.
- [2] M. Diem, M. Fisk and J. Goldman, Thin solid films, 107 (1983) 39.
- [3] C.M. Melliar-Smith, A.C. Adams, R.H. Kaiser, R.A. Kushner, J. Electrochem. Soc. 121 (1974) 298.
- [4] H. Cheung, The third international conference on chemical vapor deposition, editor F.A. Glaski, The American Nuclear Society, Hinsdale (1972), 136-142.

TASK LEADER

Marc PLISSONNIER

DRT/DTEN/SMP/LPTS
CEA Grenoble
17, rue des Martyrs
38054 Grenoble Cedex 9

Tél. : 33 4 38 78 33 42
Fax : 33 4 38 78 46 21

E-mail :plissonnier @chartreuse.cea.fr

Task Title : THERMO-MECHANICAL MODELS

INTRODUCTION

The general objective of this task is :

- to propose criterions and models which could be used in the operating conditions of high heat flux components in order to establish for each proposal its potential in terms of performances and lifetime,
- to perform studies, analysis and assessments related to thermo-mechanics for the plasma-facing component protection system (tiles, attachments) of present day tokamak.

2001 ACTIVITIES

RULES FOR DESIGN, FABRICATION AND INSPECTIONS

In fusion reactor components, rupture conditions can be achieved under series of thermal shocks. A particular simplified rule has been developed: the σ_d criterion, which takes into account thermal loading. Thermal fatigue tests with RAFM steel like 9%Cr material are necessary to validate the criterion but such tests were not found in the literature. A thermal fatigue test has been designed in 2001 and the feasibility of this test is studied on 316L specimens: the constitution of the test bench is already realised and test is now ongoing.

TILES INTEGRITY

A preliminary study on the choice of a tile integrity criterion has been conducted for carbon fibres reinforced carbon composites (CFC's): this criterion could be used in the operating conditions as parameters in order to establish for each proposal its potential in terms of performances and lifetime.

CONCLUSIONS

RULES FOR DESIGN, FABRICATION AND INSPECTIONS

A thermal fatigue test has been designed: the constitution of the test bench is already realised and test is now ongoing on a 316L specimen.

The picture below presents the experiment (with a not fixed pipe).



Test bench

A 3D finite element modelling has been introduced to estimate the number of cycles to crack initiation and then the test duration.

The pursuit of its development will be made on the basis of the first experimental results.

The further tests will be realised on 9%Cr steel pipes and notch will be machined for the study of the initiation and propagation of a crack under thermal fatigue loading.

TILES INTEGRITY

Failure criteria for CFC materials can be used to evaluate the integrity of tiles used as plasma facing components under thermal and mechanical loads and to test the different designs.

However rupture strengths must be determine for each type of CFC material. A wide range of CFC materials can be considered for plasma facing components [1].

The mechanical properties (which depend on raw materials, process and structure) are specific to each composite and may differ highly from a composite to another. For instance, values of the tensile strength reported in literature for CFC composites in the fibres direction ranges from 30 to more than 380 MPa.

The study indicates that two main failure macroscopic failure theories can be used for CFC materials. Values of fracture strength in tension, compression and shear for the different directions (plus eventually interaction terms) must be known to use these criteria.

A complete set of data corresponding to a three dimensional composite [2] will be used to evaluate the integrity of a tile submitted to thermal and mechanical loads.

REFERENCES

- [1] P. G. Valentine et al. Journal of nuclear materials 233-237 (1996) 660-666.
- [2] L. Moncel, 'Etude des mécanismes d'endommagement d'un assemblage cuivre/composite carbone-carbone sous chargement thermomécanique'. Thèse soutenue le 18 Juin 1999. Rapport EUR-CEA-FC-1682.

REPORTS AND PUBLICATIONS

Ph. Matheron, "Progress in the design and construction of a thermal fatigue experimental set-up", CEA report DM2S SEMT/LISN/RT/02-009/A (February, 8, 2002).

C. Guerin "Failure criteria for carbon fiber reinforced carbon composite (CFC)", CEA report DM2S to be published.

C. Guerin "Integrity evaluation of a CFC tile under thermo-mechanical loading – A finite element calculation using CAST3M", CEA report DM2S to be published.

TASK LEADER

Laetitia NICOLAS

DEN/DM2S/SEMT
CEA Saclay
91191 Gif-sur-Yvette Cedex

Tél. : 33 1 69 08 55 40
Fax : 33 1 69 08 86 84

E-mail : laetitia.nicolas@cea.fr